Supporting Information

Design and Construction of a Chiral Cd(II)-MOF From Achiral Precursors: Synthesis, Crystal Structure and Catalytic Activity Towards C-C and C-N Bond Forming Reactions

Vijay Gupta and Sanjay K. Mandal*

Department of Chemical Sciences, Indian Institute of Science Education and Research Mohali, Sector 81, Manauli PO, S.A.S. Nagar, Mohali Punjab 140306, INDIA

*Author for correspondence:
Prof. Sanjay K. Mandal, E-mail: sanjaymandal@iisrmohali.ac.in.

Table of Contents

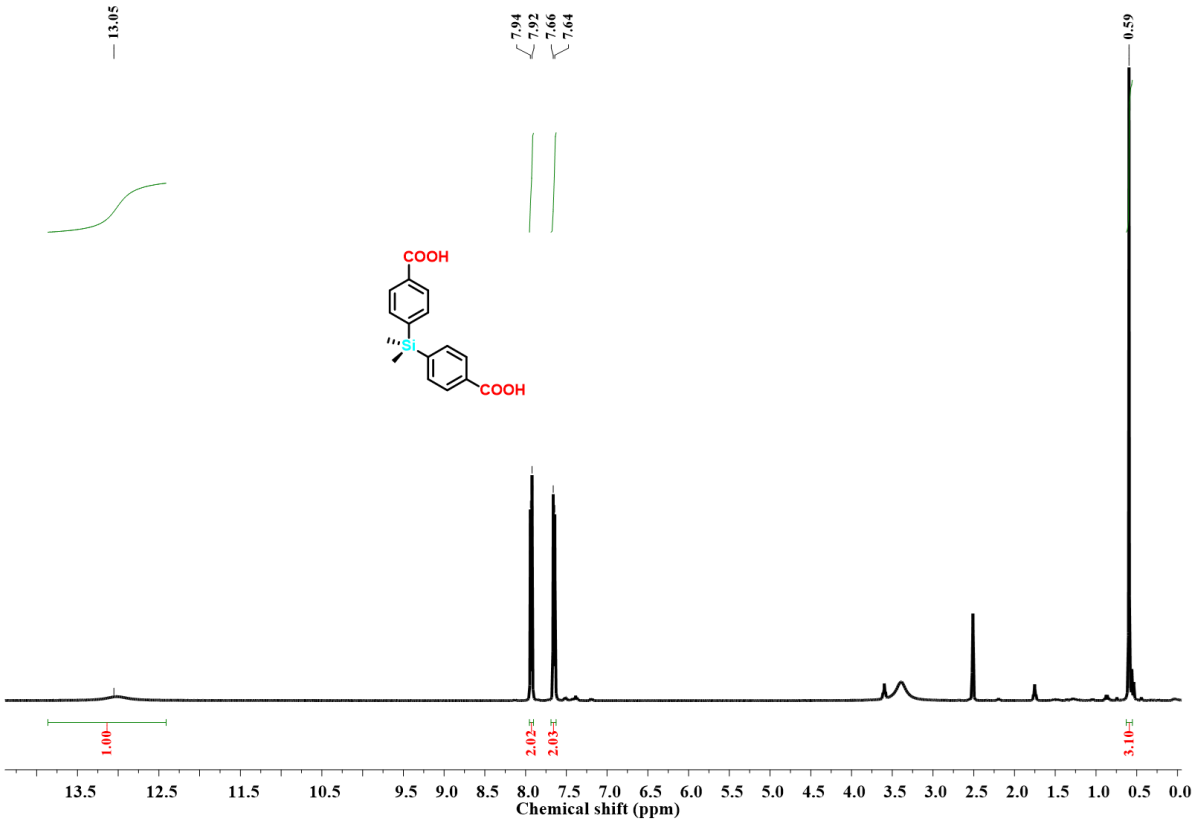

Figure S1. ^{1}H NMR spectrum of H_2L in DMSO-d_6.

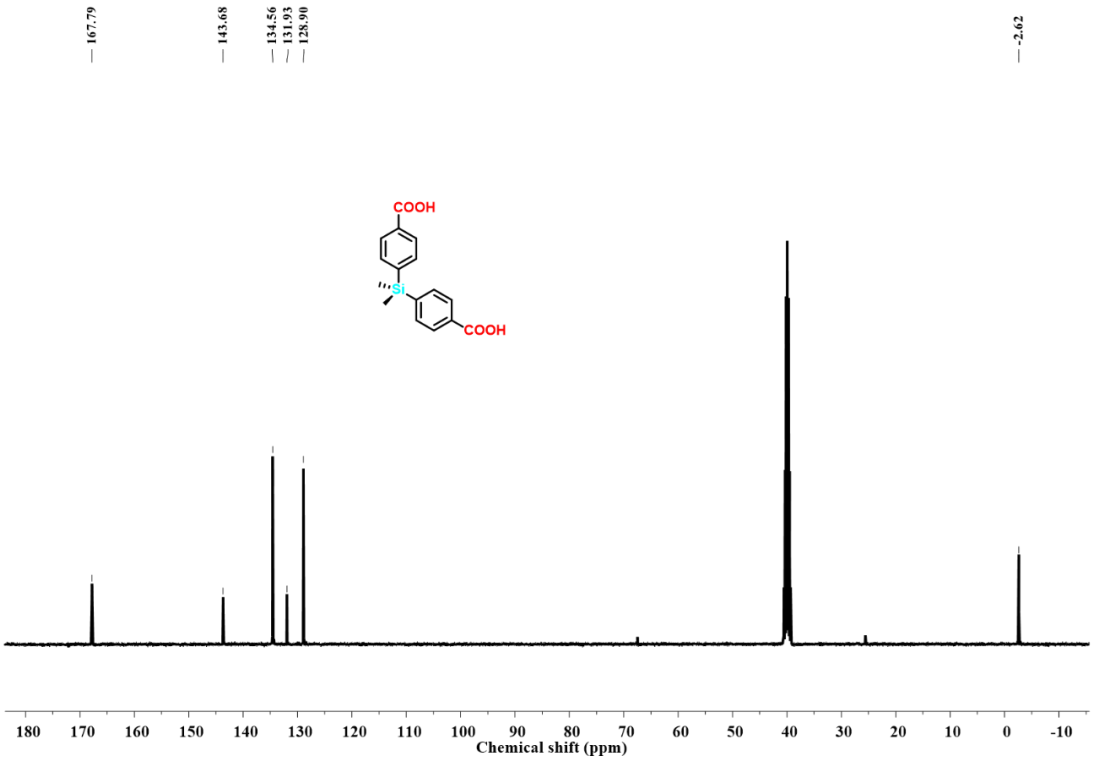

Figure S2. ^{13}C NMR spectrum of H_2L in DMSO-d_6.

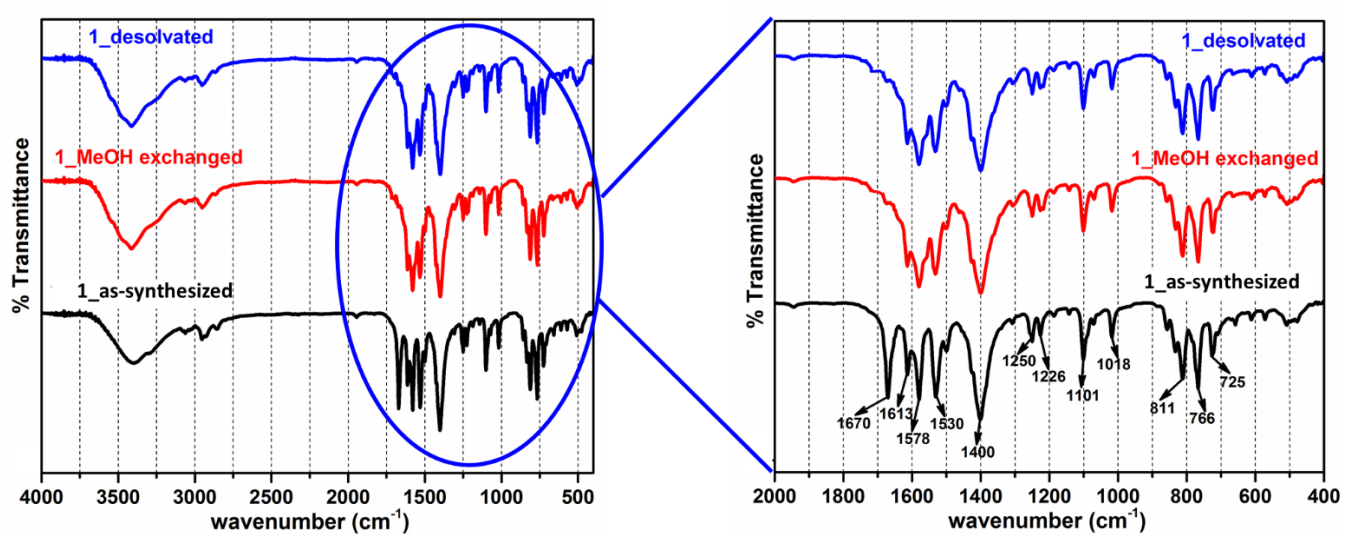

Figure S3. FTIR spectra for the as-synthesized, methanol exchanged and desolvated **1**, indicating loss of lattice DMF and coordinated water upon activation.

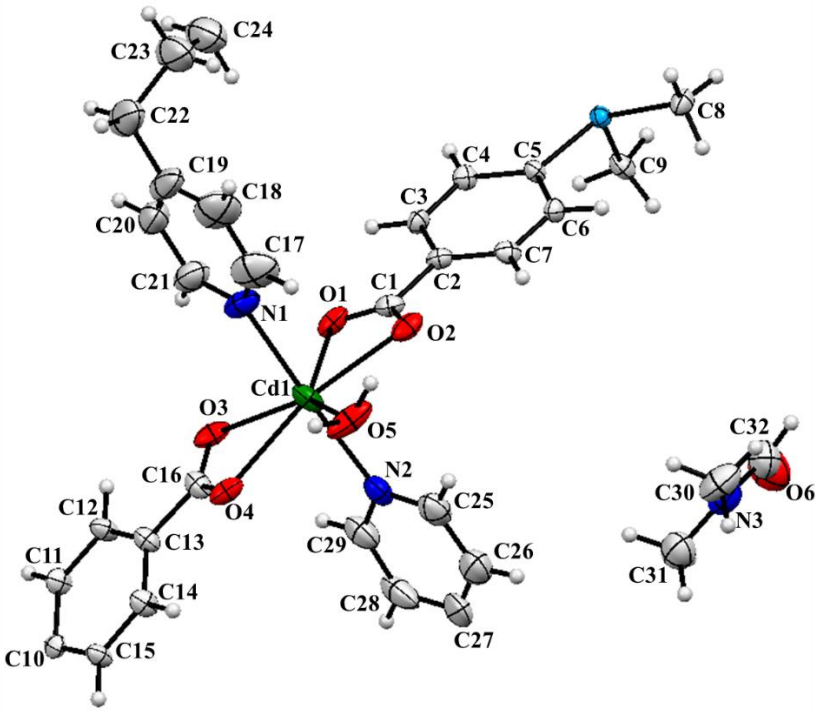

Figure S4. An ORTEP view of the asymmetric unit in **1**.

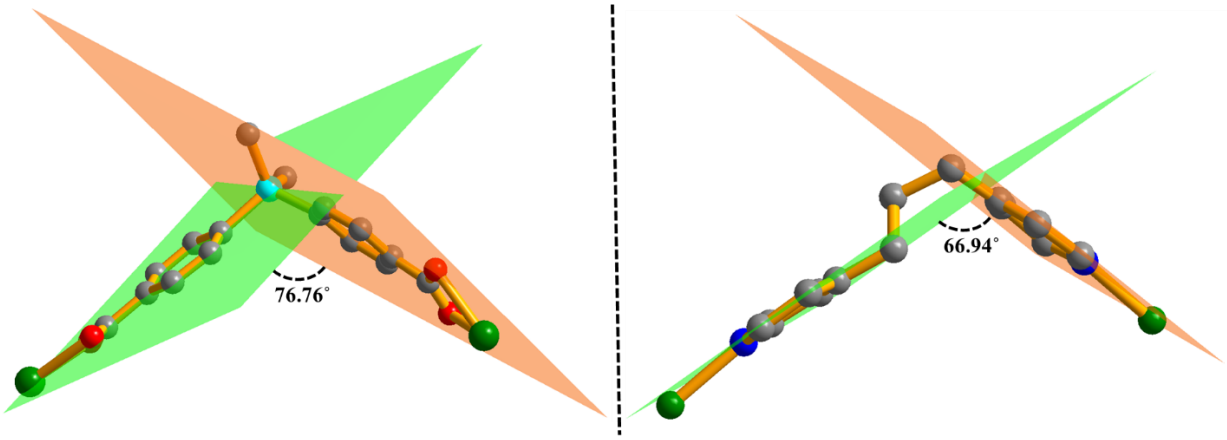

Figure S5. Angles between the two phenyl rings (left) and pyridyl rings (right) in the ligands H_2L and bpp, respectively, in **1**.

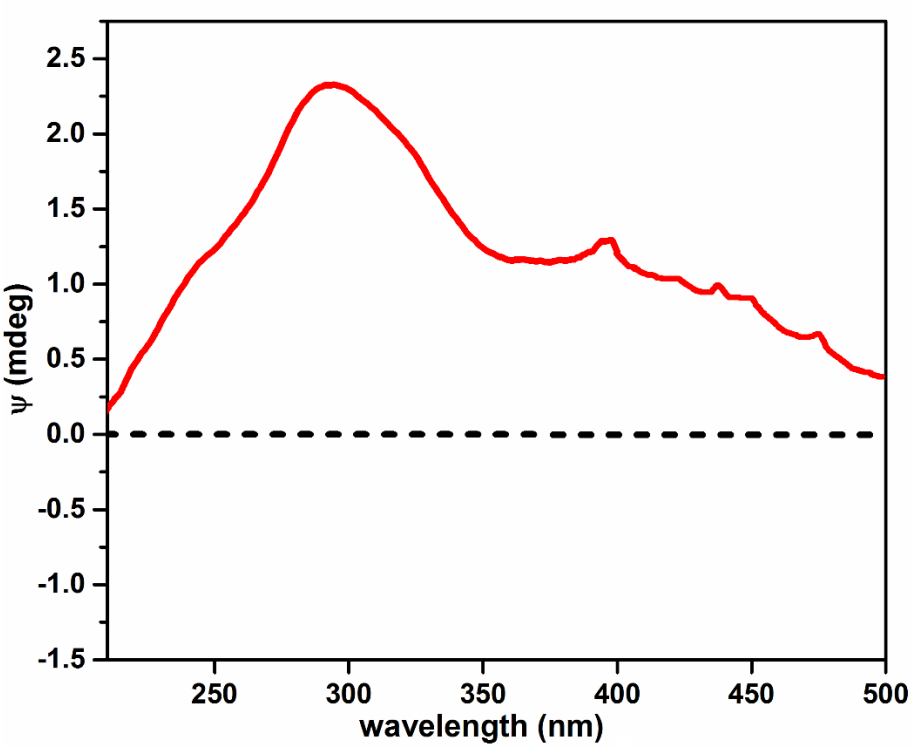

Figure S6. Solid State Circular Dichroism (CD) spectrum for **1**.

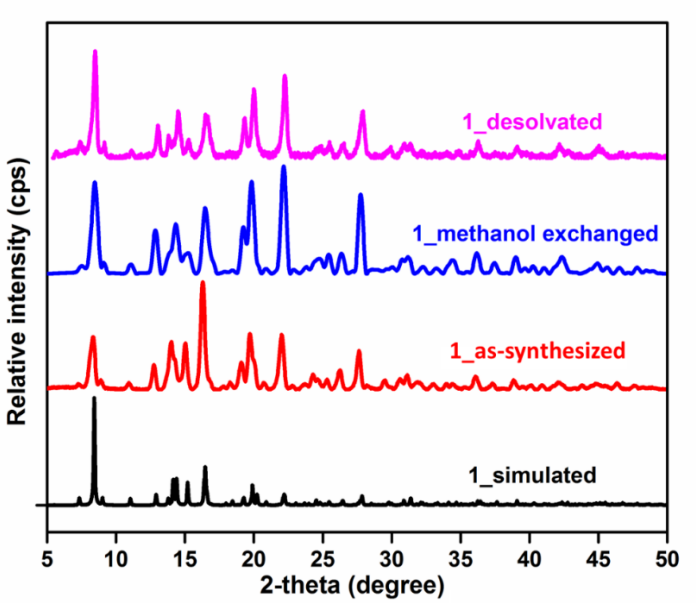

Figure S7. Powder X-ray diffraction (PXRD) patterns of the as-synthesized, methanol exchanged and desolvated **1** compared with the simulated powder pattern obtained from the single crystal X-ray data.

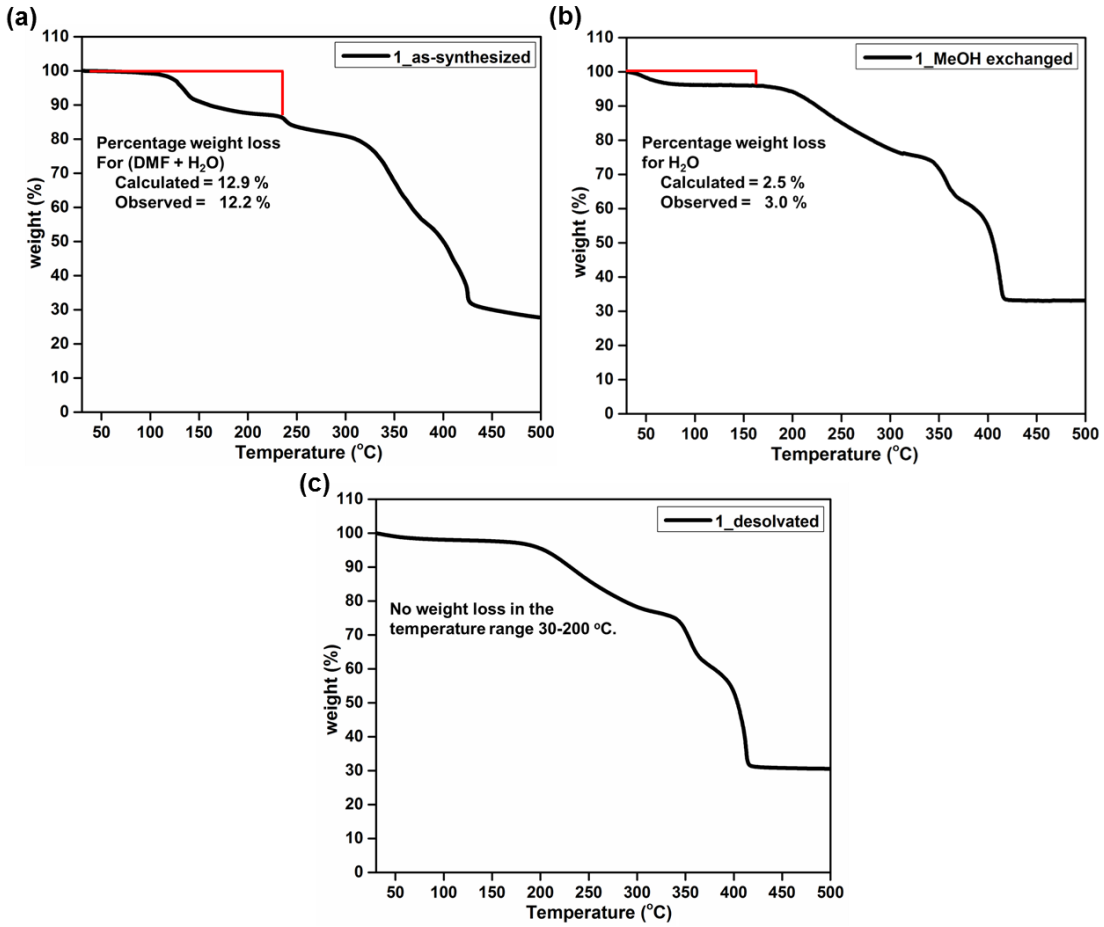

Figure S8. Thermogravimetric profiles for (a) as-synthesized **1**, (b) methanol-exchanged **1** and (c) the desolvated **1**.

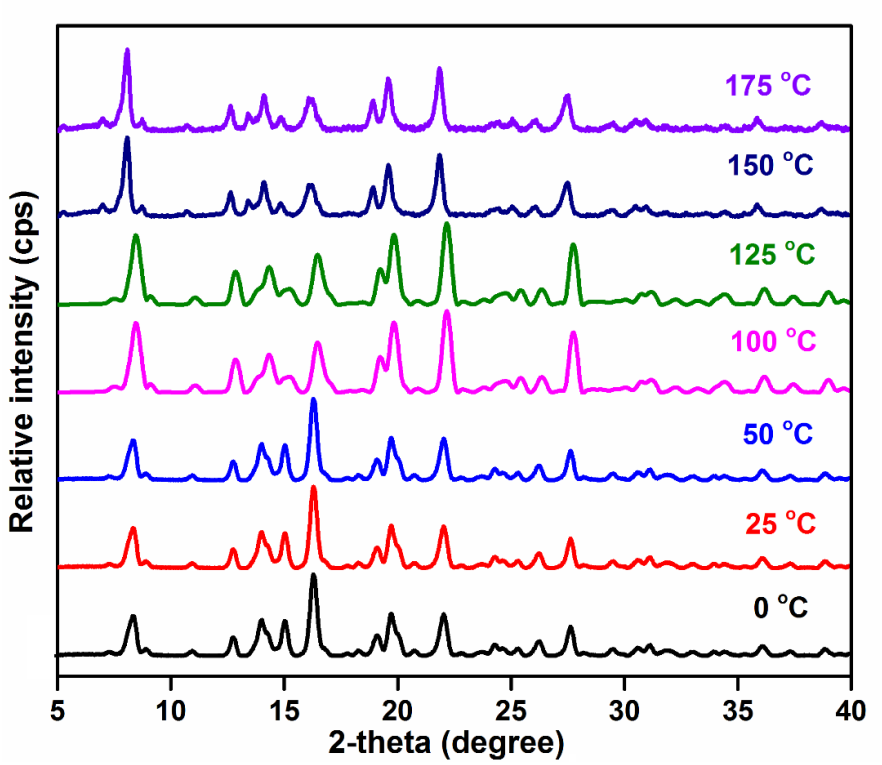

Figure S9. In-situ variable temperature powder X-ray diffraction pattern of the as-synthesized **1**.

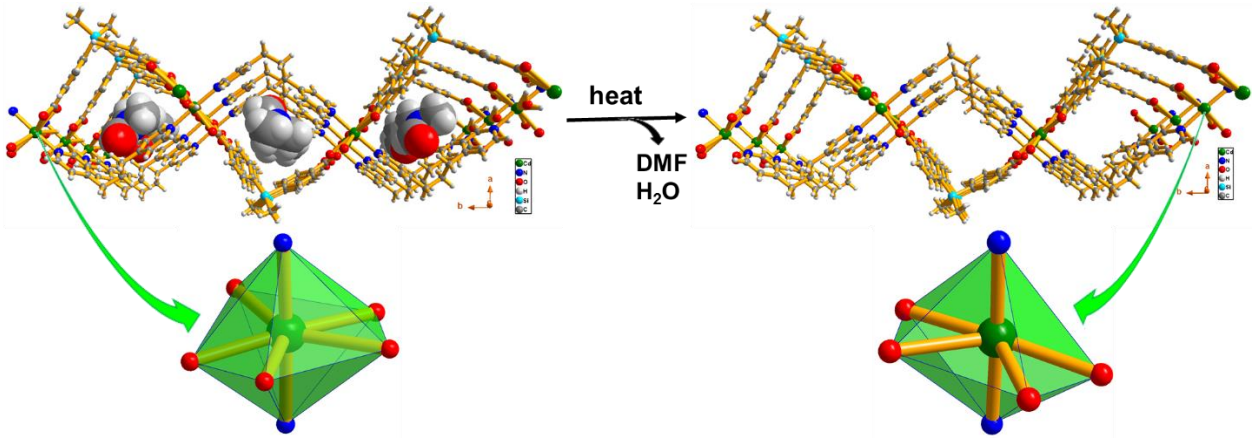

Figure S10. Schematic representation for the generation of open pores and active metal center in **1** through thermal treatment.

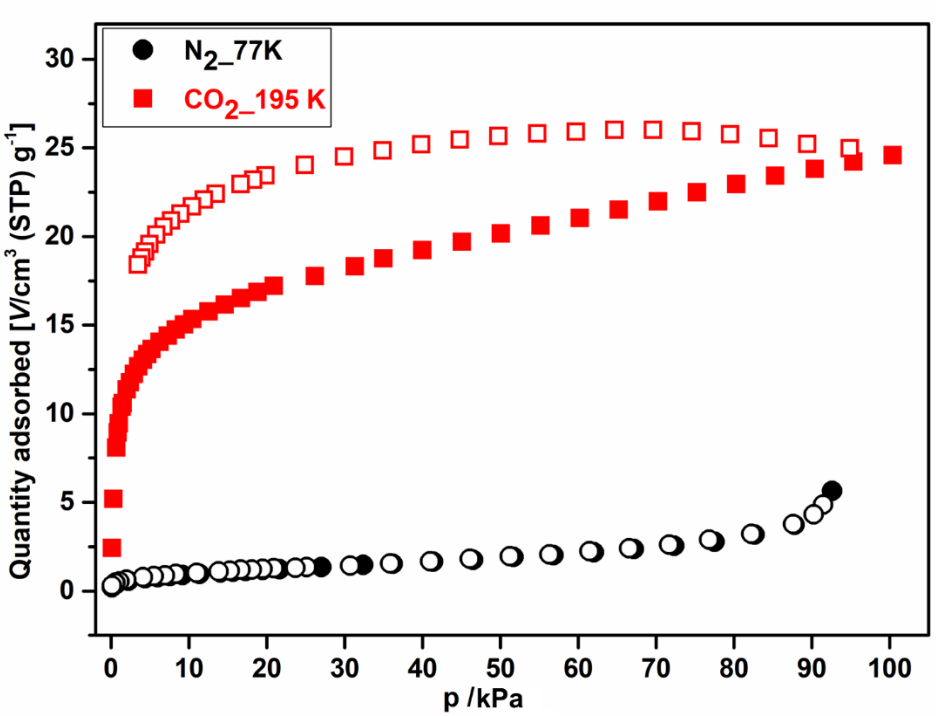

Figure S11. N_2 and CO_2 sorption isotherms for **1**, at 77 K and 195 K, respectively. Filled circles and open circles indicates the adsorption and desorption points, respectively.

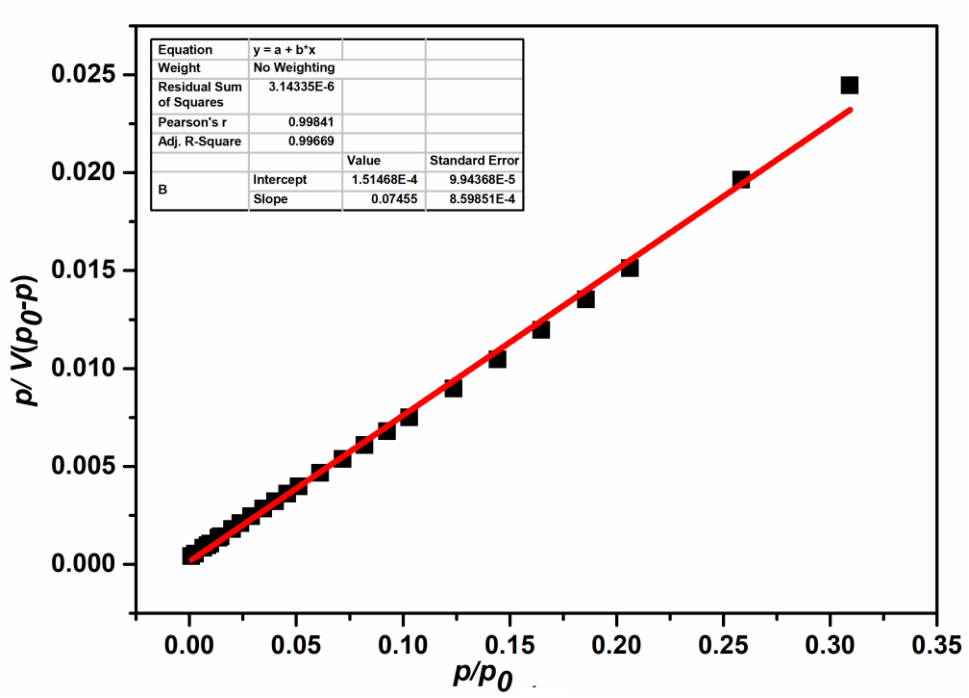

S_{BET} = {[1 / (0.07455 + 0.000151468)] / 22414} x 6.023 x 10^{23} x 0.170 x 10^{-18} = 61 m^2g^{-1}.

Figure S12. BET surface area of **1** obtained from the CO_2 adsorption isotherm at 195 K.

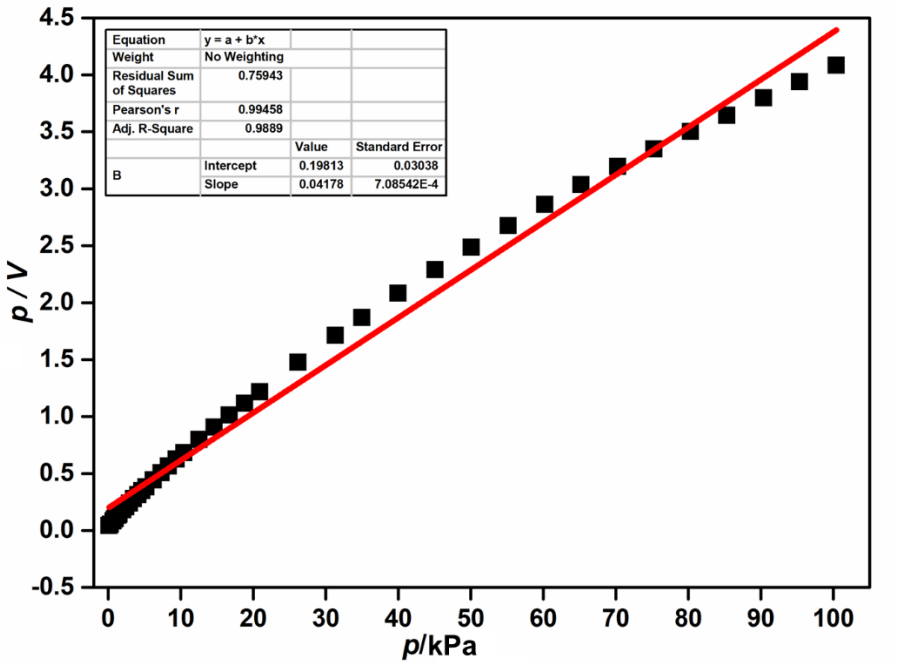

$S_{Langmuir}$ = [(1 / 0.04178) / 22414] x 6.023 x 10^{23} x 0.170 x 10^{-18} = 109 m^2g^{-1}.

Figure S13. Langmuir surface area of **1** obtained from the CO_2 adsorption isotherm at 195 K.

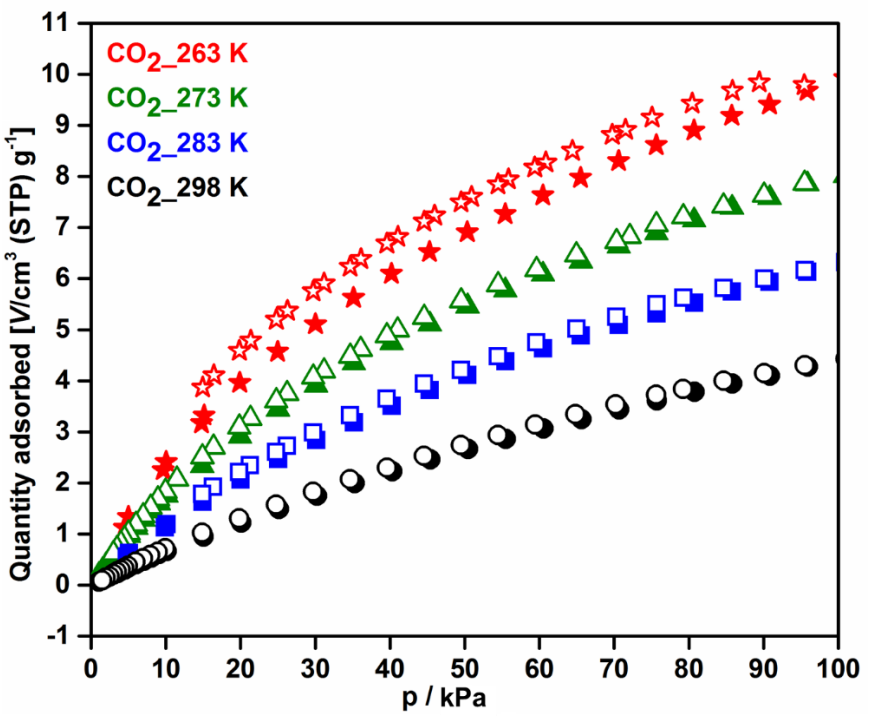

Figure S14. CO_2 sorption isotherms at different temperatures for **1**.

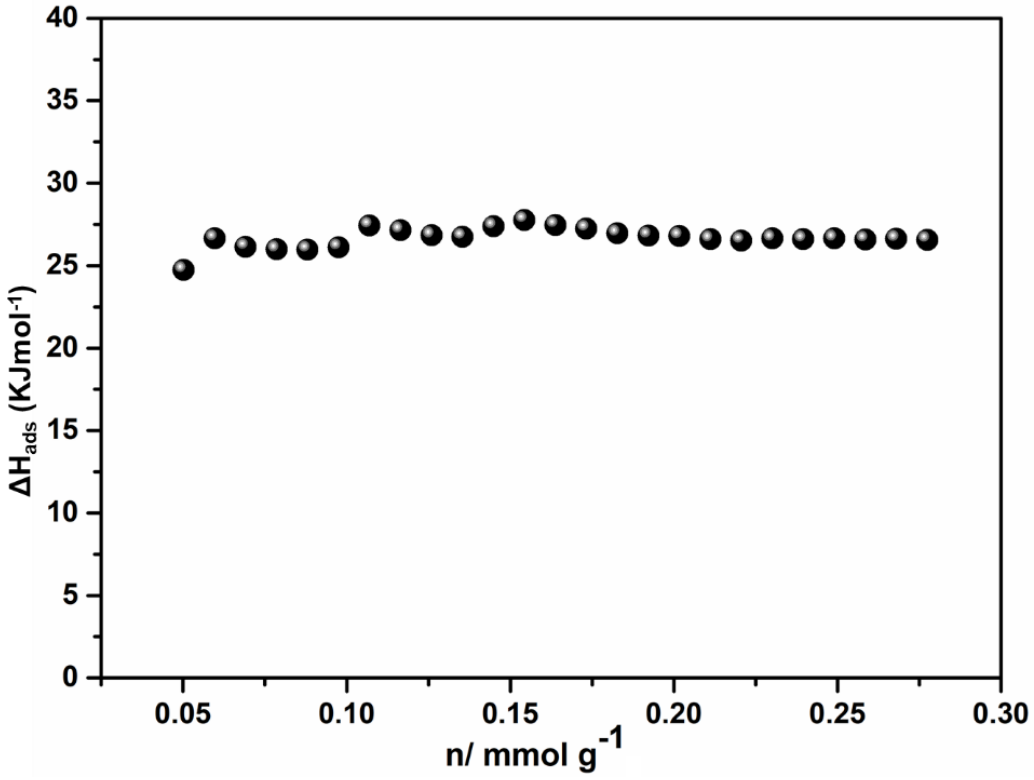

Figure S15. Variation of isosteric heat of adsorption calculated from the CO_2 isotherms of **1** at four different temperatures with respect to its surface coverage.

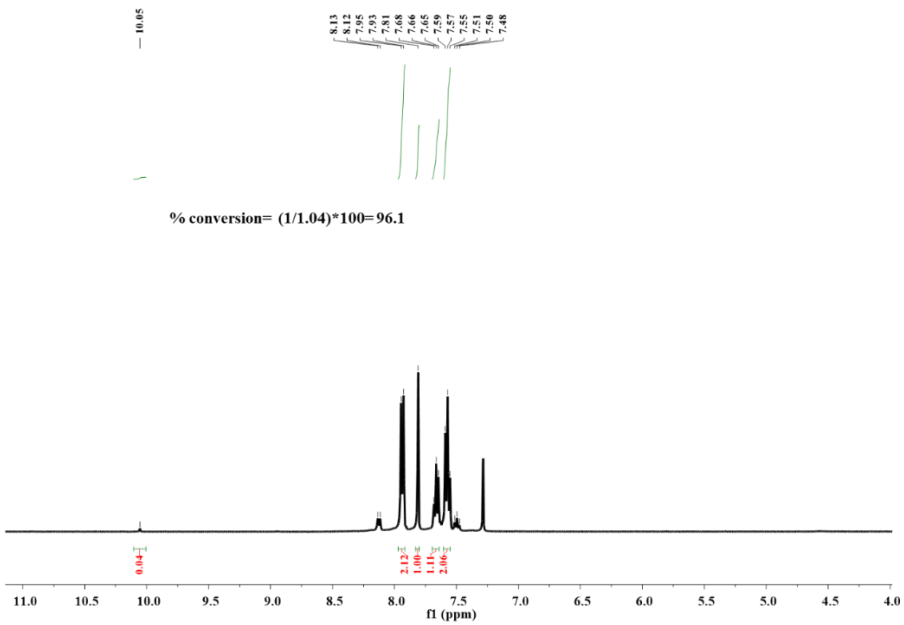

Figure S16. Example of integration in the ^{1}H NMR spectrum for the determination of percent conversion in the Knoevenagel condensation reaction of benzaldehyde with malononitrile (Table 1, entry 1).

Calculation of percent conversion in the Knoevenagel condensation reaction of benzaldehyde with malononitrile catalyzed by 1

Total amount of compounds at the end (see Figure S16):

Unreacted bezaldehyde (10.05 ppm) + 2-benzylidenemalononitrile (7.81 ppm) = 0.04 + 1.00 = 1.04

Yield of 2-benzylidenemalononitrile = (1/1.04) * 100 = 96.1 %.

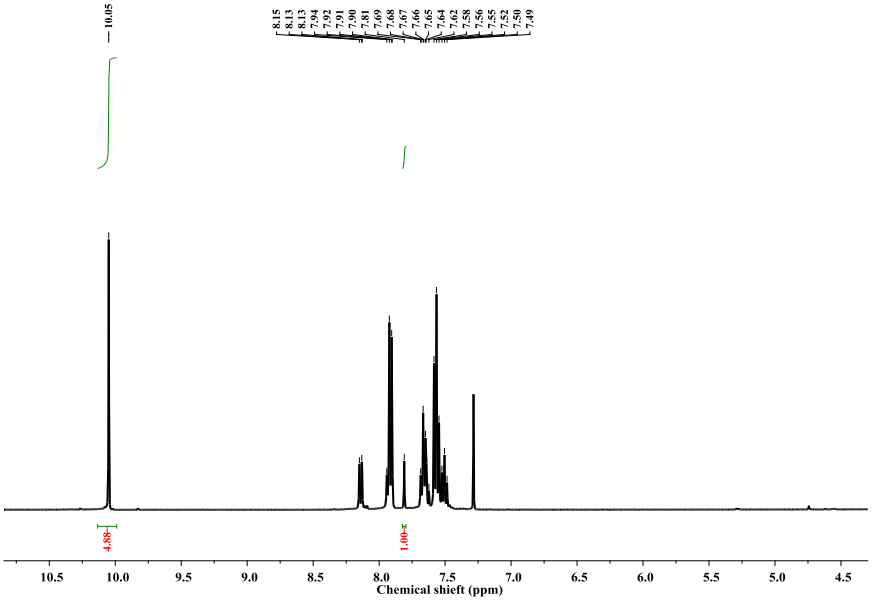

Figure S17. ^{1}H NMR spectrum (in $CDCl_3$) for Knoevenagel condensation reaction of benzaldehyde with malononitrile in absence of any catalyst (Table 1, entry 15).

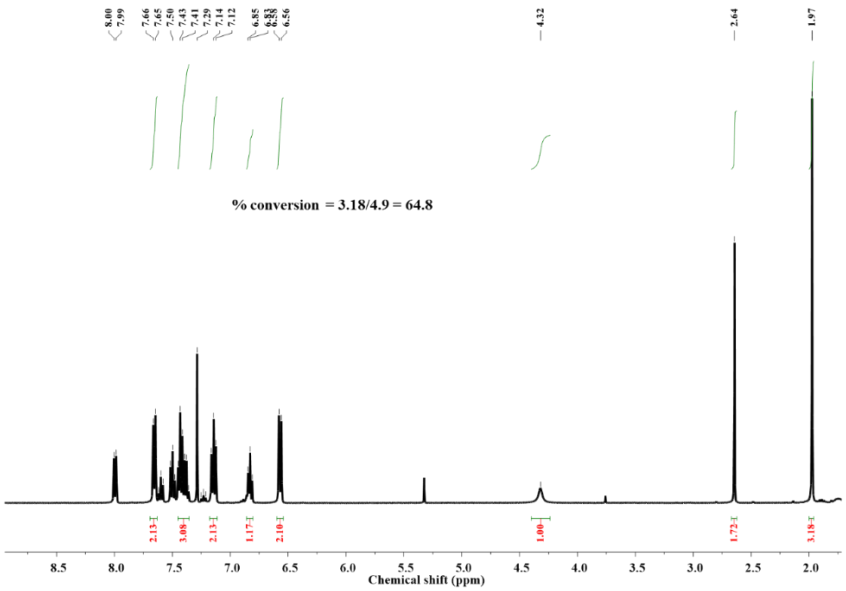

Figure S18. Example of integration in the ^{1}H NMR spectrum for the determination of percent conversion in Strecker reaction of acetophenone with aniline and trimethylsilyl cyanide (Table 2, entry 4).

Calculation of product yield in the Strecker reaction of acetophenone with aniline and trimethylsilyl cyanide (TMSCN) catalyzed by 1

Total amount of compounds at the end (see Figure S17):

Unreacted acetophenone (2.64 ppm) + 2-phenyl-2-(phenylamino)propanenitrile (1.97 ppm) = 1.72 + 3.18 = 4.9

Yield of 2-benzylidenemalononitrile = (3.18/4.9) * 100 = 64.8 %.

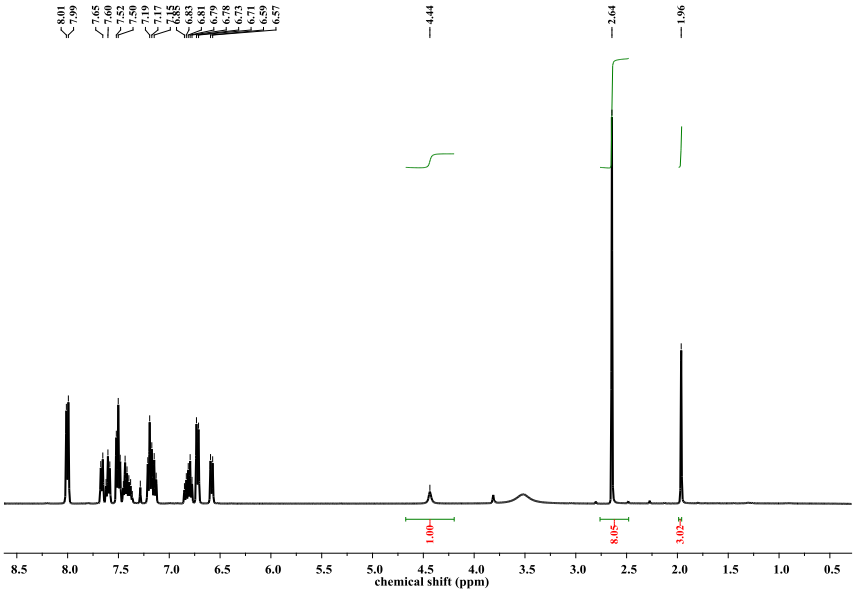

Figure S19. ^{1}H NMR spectrum (in $CDCl_3$) for Strecker reaction of acetophenone with aniline and trimethyl silyl cyanide in absence of any catalyst (Table 2, entry 14).

NMR spectra of the isolated products from the Knoevenagel reaction:

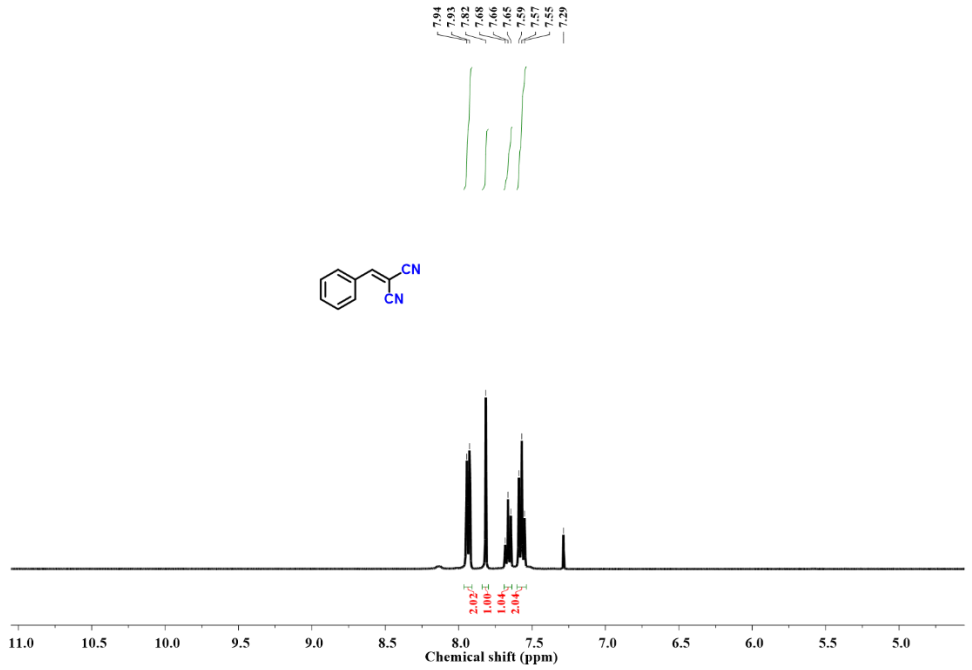

Figure S20. ^{1}H NMR spectrum of benzylidene malononitrile (Table 1, entry 1) in $CDCl_3$.

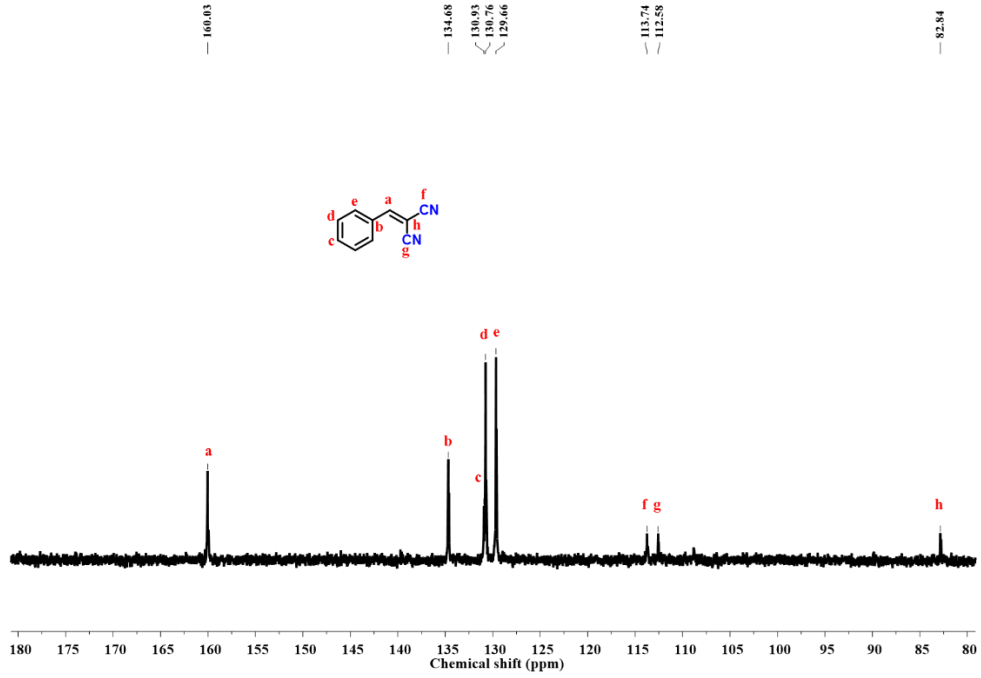

Figure S21. ^{13}C NMR spectrum of benzylidene malononitrile (Table 1, entry 1) in $CDCl_3$.

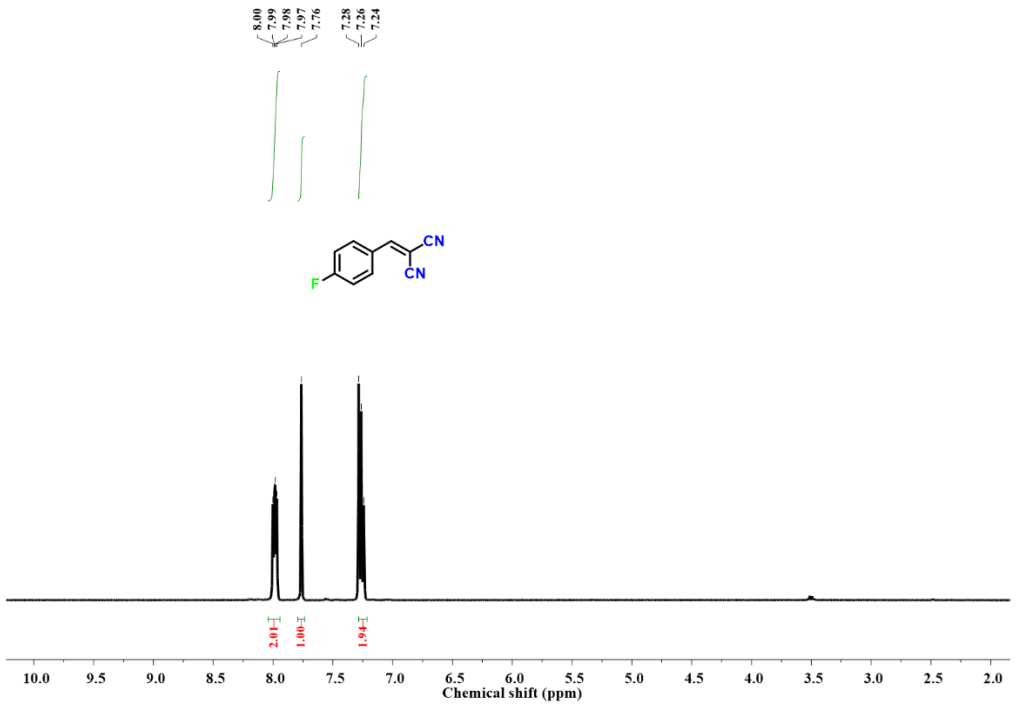

Figure S22. ^{1}H NMR spectrum of 2-(4-fluorobenzylidene)malononitrile (Table 1, entry 2) in $CDCl_3$.

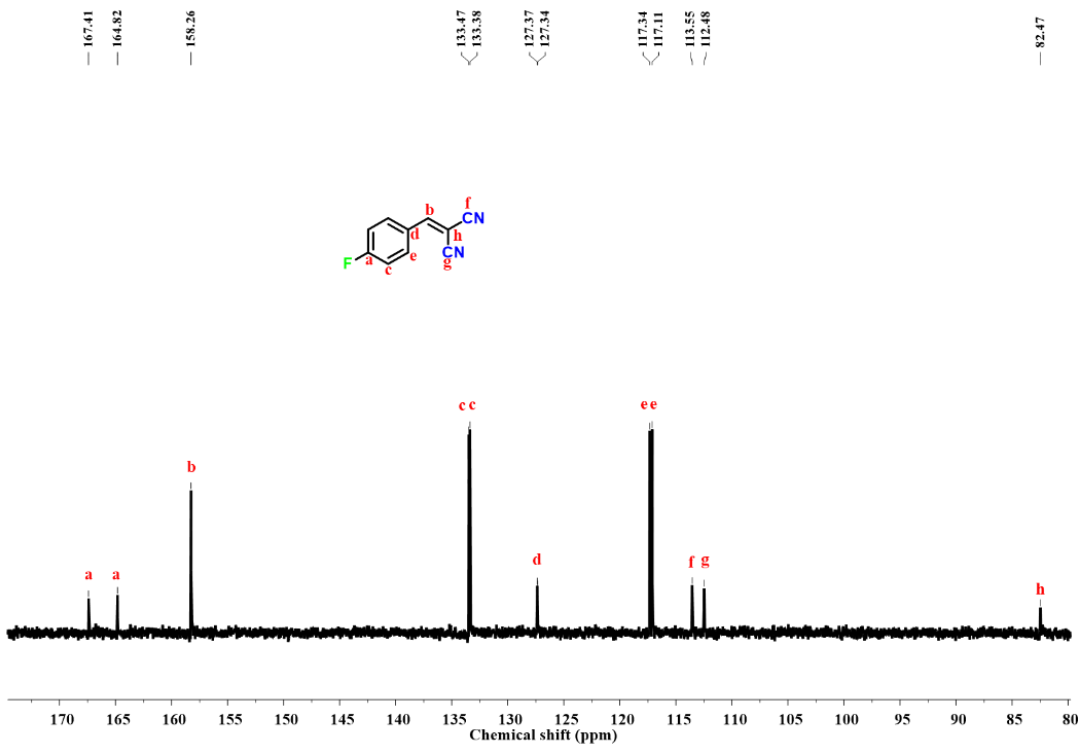

Figure S23. ^{13}C NMR spectrum of 2-(4-fluorobenzylidene)malononitrile (Table 1, entry 2) in $CDCl_3$.

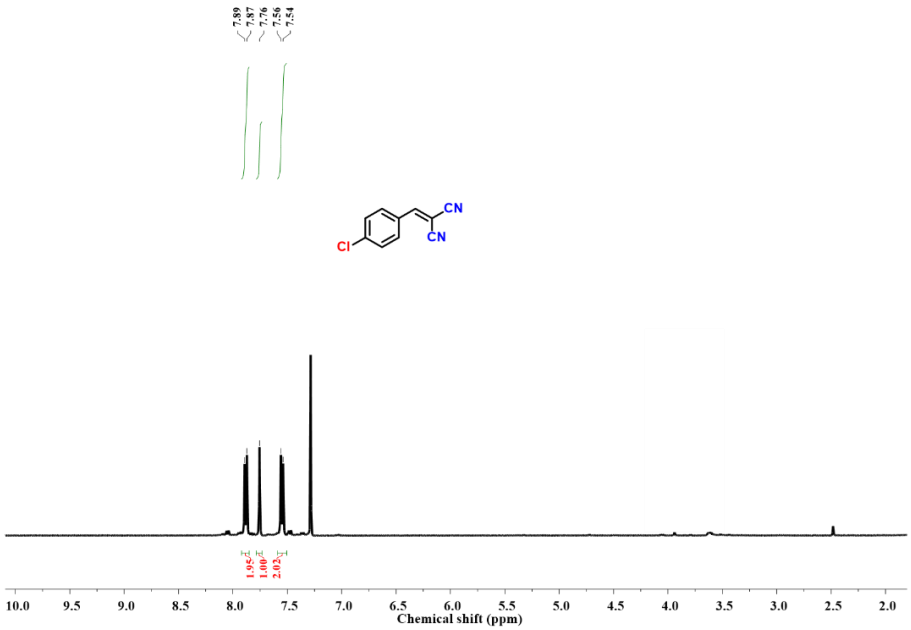

Figure S24. ^{1}H NMR spectrum of 2-(4-chlorobenzylidene)malononitrile (Table 1, entry 3) in $CDCl_3$.

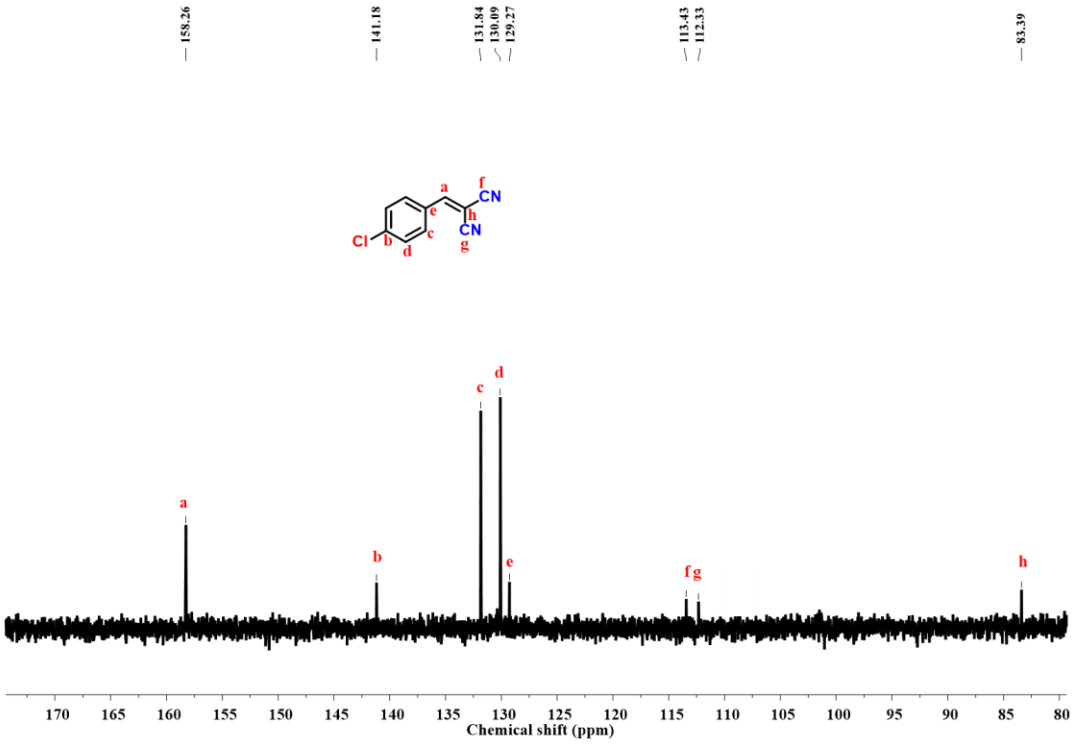

Figure S25. ^{13}C NMR spectrum of 2-(4-chlorobenzylidene)malononitrile (Table 1, entry 3) in $CDCl_3$.

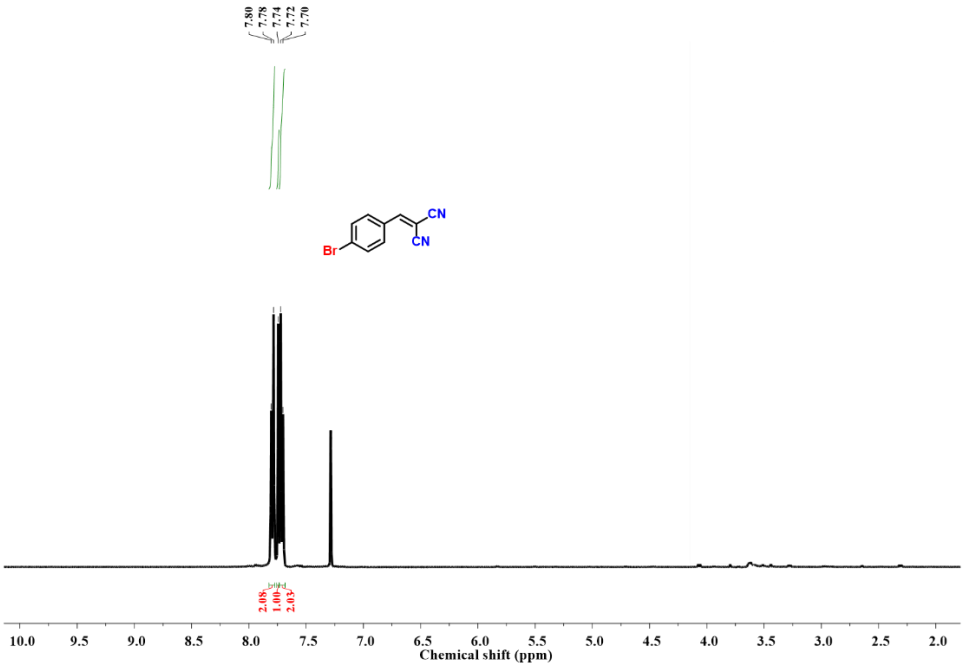

Figure S26. ^{1}H NMR spectrum of 2-(4-bromobenzylidene)malononitrile (Table 1, entry 4) in $CDCl_3$.

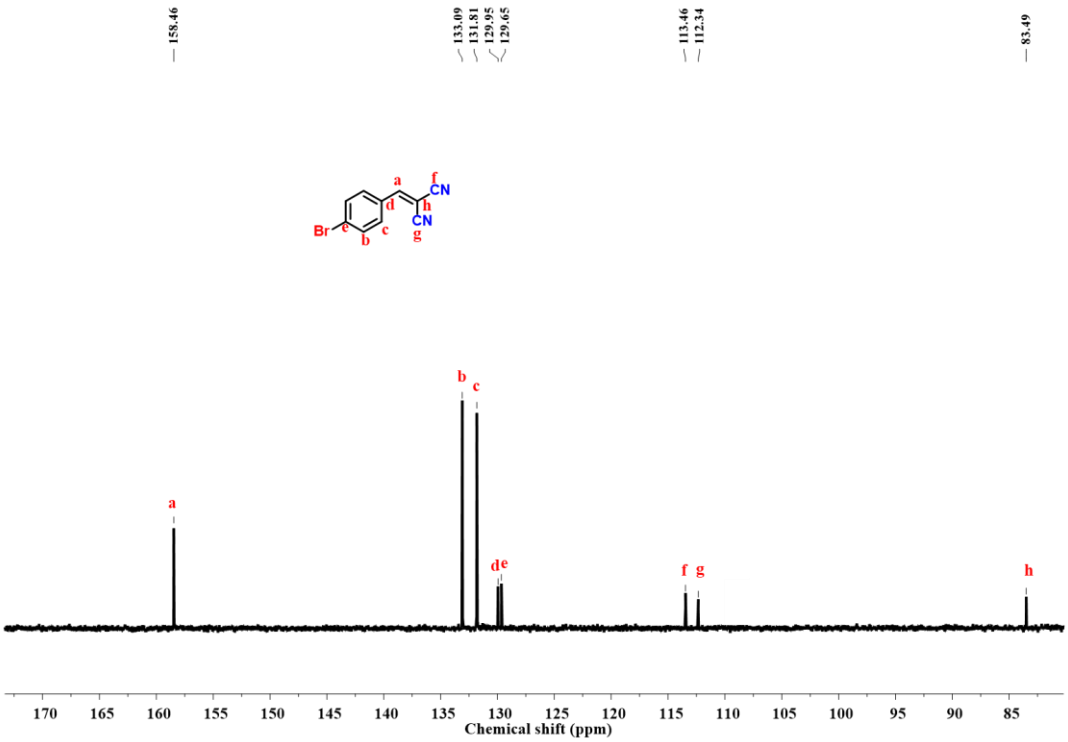

Figure S27. ^{13}C NMR spectrum of 2-(4-bromobenzylidene)malononitrile (Table 1, entry 4) in $CDCl_3$.

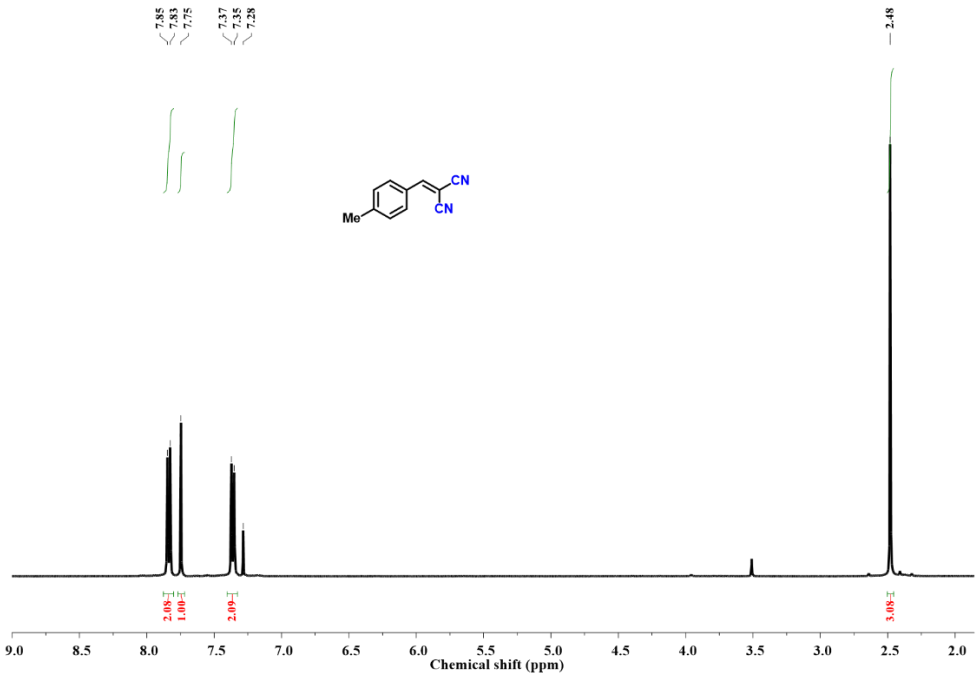

Figure S28. ^{1}H NMR spectrum of 2-(4-methylbenzylidene)malononitrile (Table 1, entry 5) in $CDCl_3$.

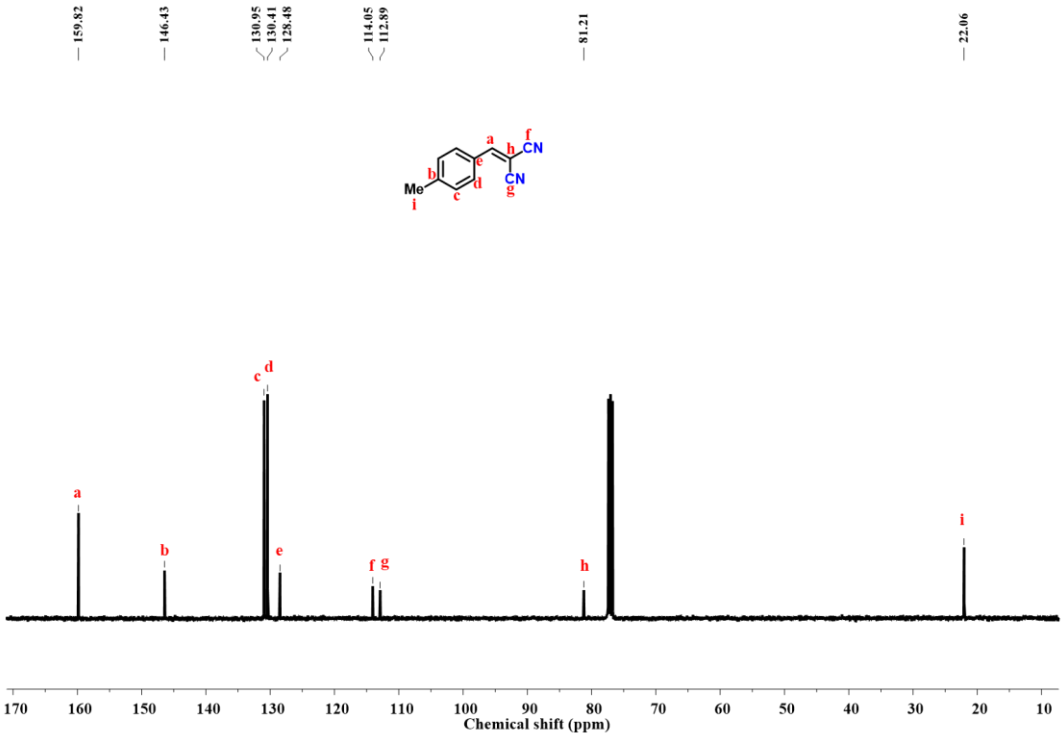

Figure S29. ^{13}C NMR spectrum of 2-(4-methylbenzylidene)malononitrile (Table 1, entry 5) in $CDCl_3$.

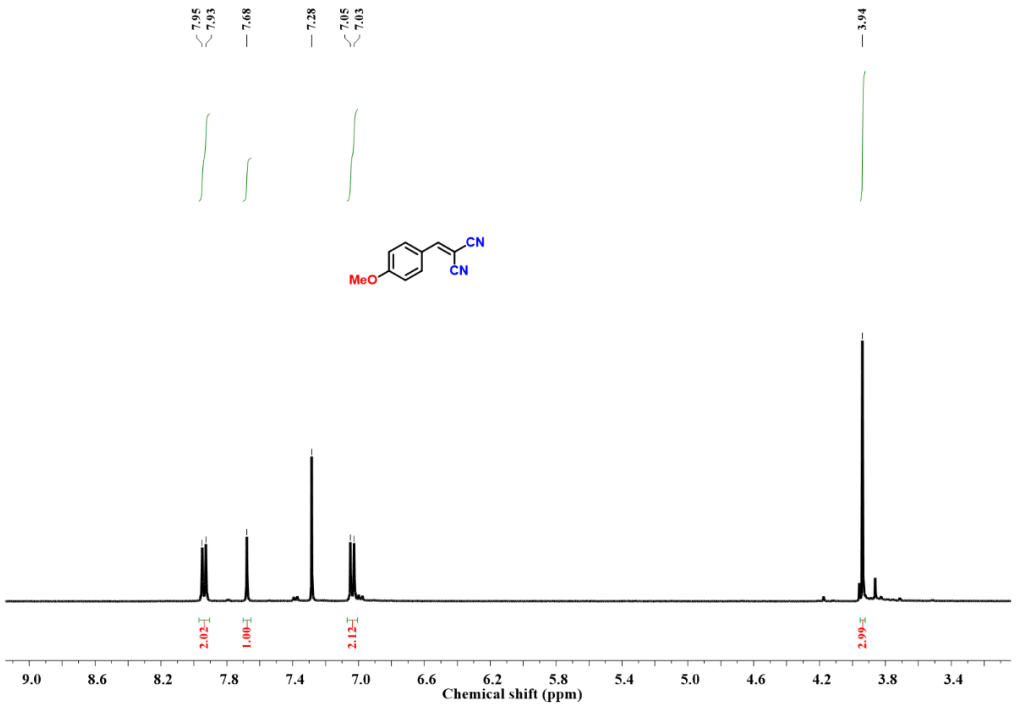

Figure S30. ^{1}H NMR spectrum of 2-(4-methoxybenzylidene)malononitrile (Table 1, entry 6) in $CDCl_3$.

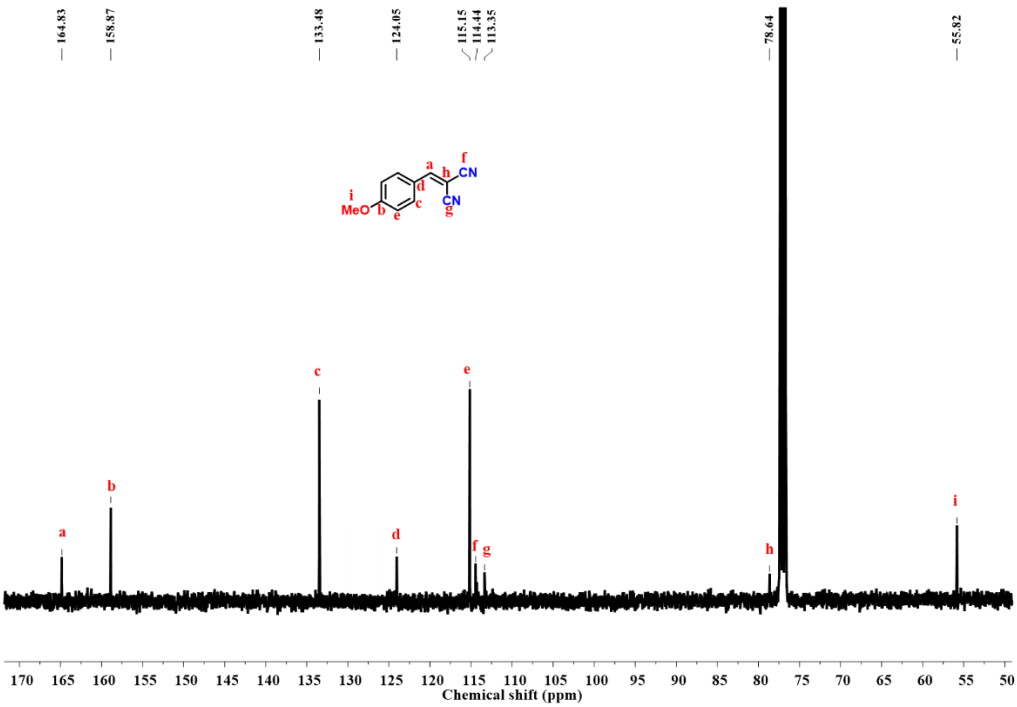

Figure S31. ^{13}C NMR spectrum of 2-(4-methoxybenzylidene)malononitrile (Table 1, entry 6) in $CDCl_3$.

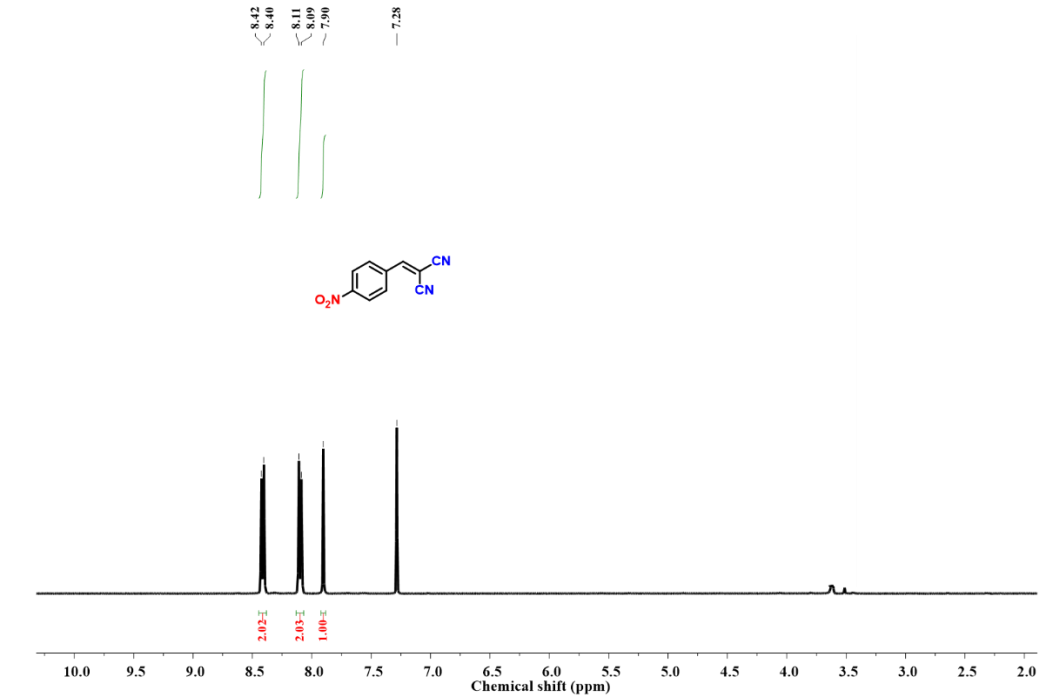

Figure S32. ^{1}H NMR spectrum of 2-(4-nitrobenzylidene)malononitrile (Table 1, entry 7) in $CDCl_3$.

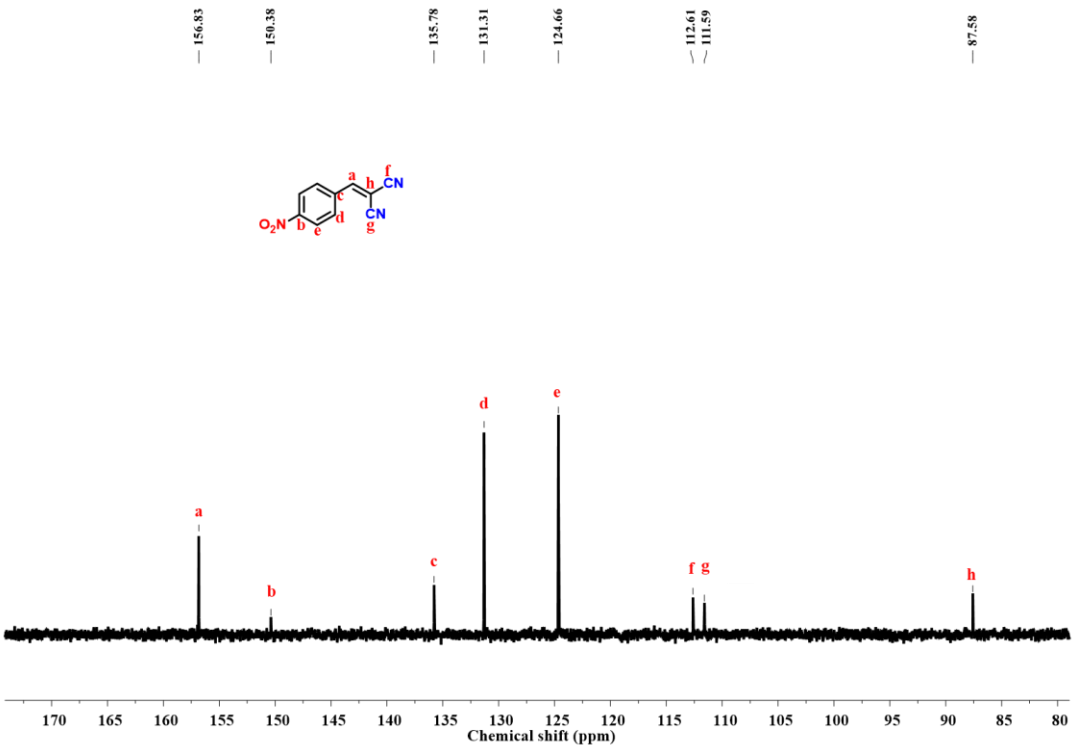

Figure S33. ^{13}C NMR spectrum of 2-(4-nitrobenzylidene)malononitrile (Table 1, entry 7) in $CDCl_3$.

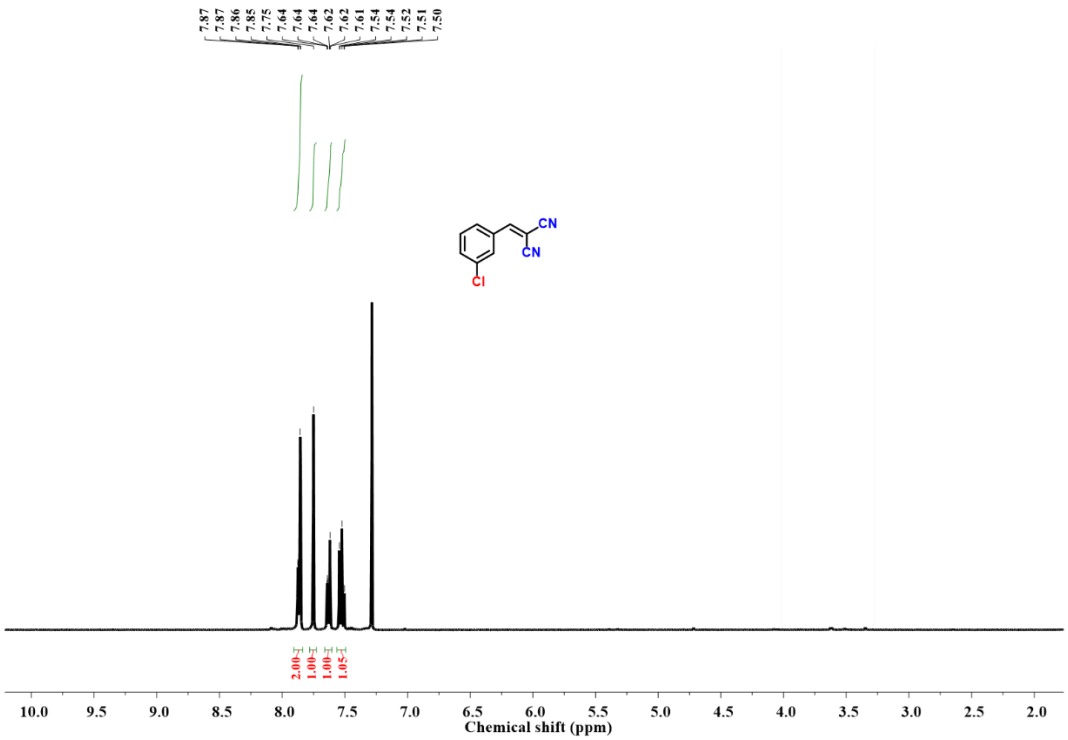

Figure S34. ^{1}H NMR spectrum of 2-(3-chlorobenzylidene)malononitrile (Table 1, entry 8) in $CDCl_3$.

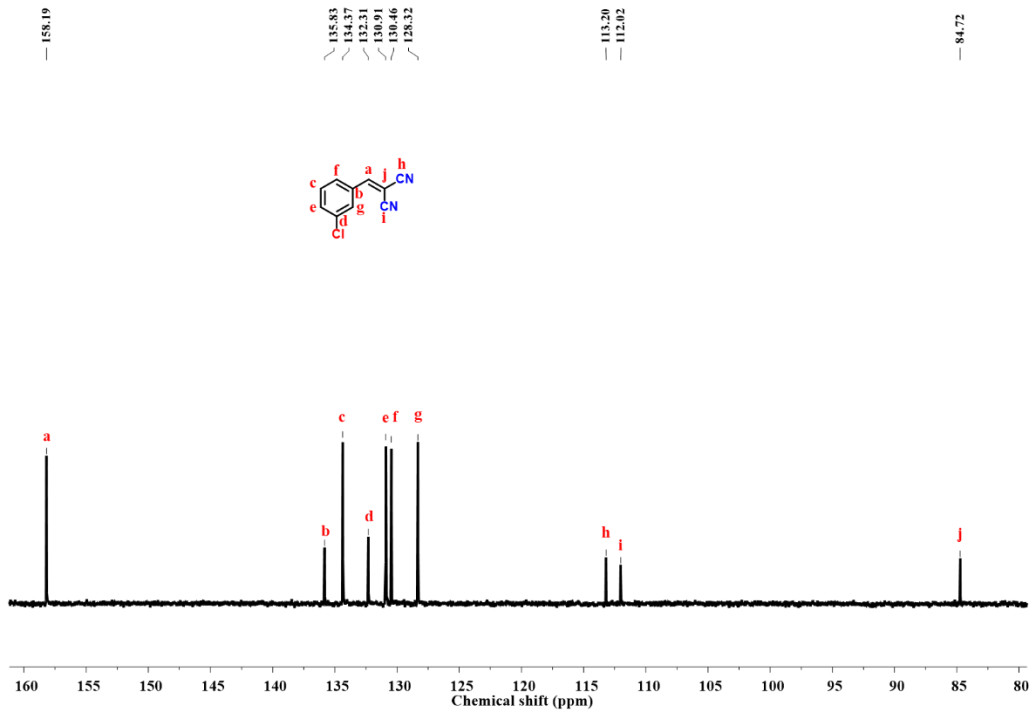

Figure S35. ^{13}C NMR spectrum of 2-(3-chlorobenzylidene)malononitrile (Table 1, entry 8) in $CDCl_3$.

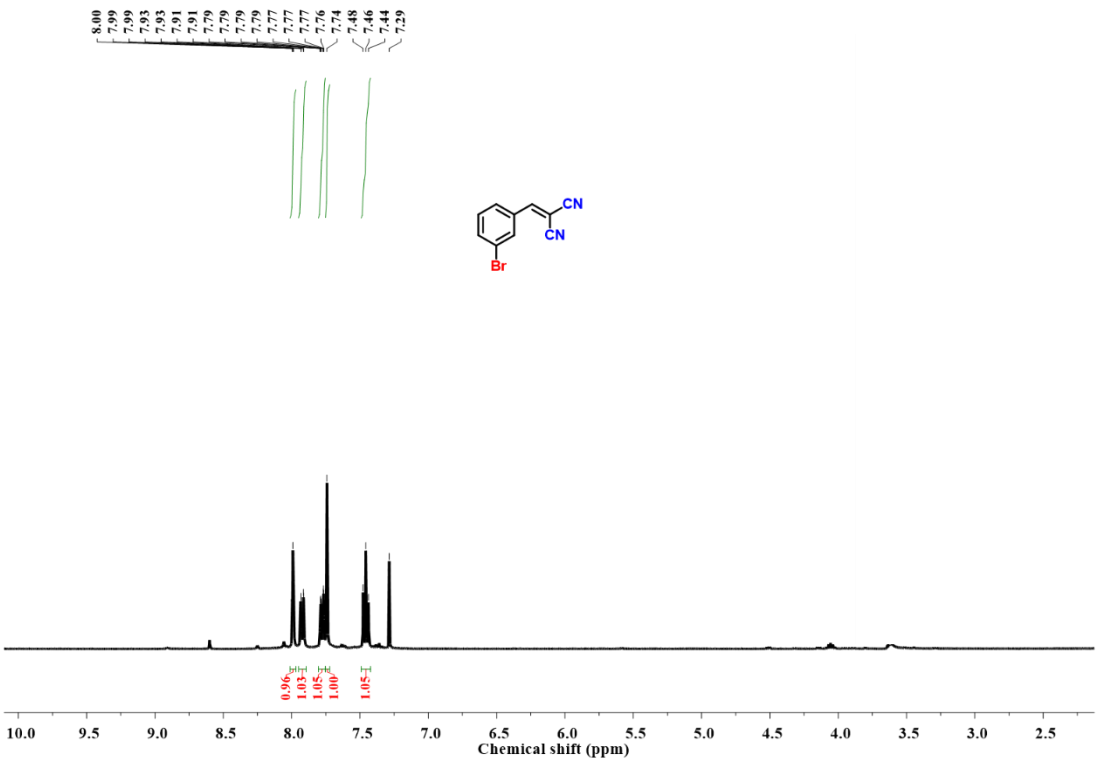

Figure S36. ^{1}H NMR spectrum of 2-(3-bromobenzylidene)malononitrile (Table 1, entry 9) in $CDCl_3$.

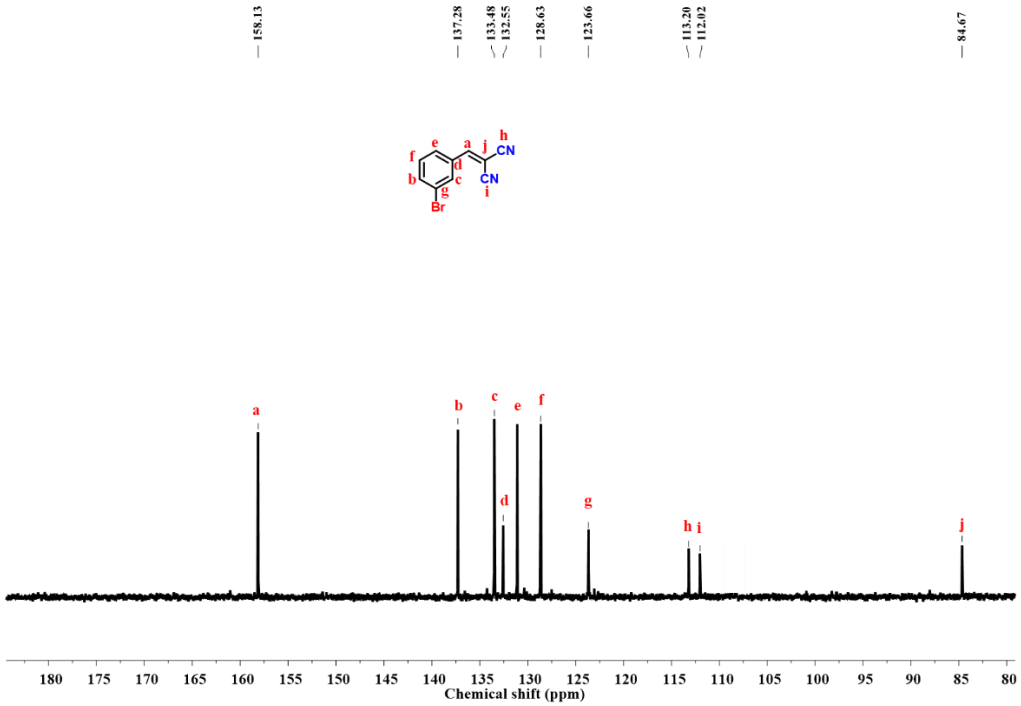

Figure S37. ^{13}C NMR spectrum of 2-(3-bromobenzylidene)malononitrile (Table 1, entry 9) in $CDCl_3$.

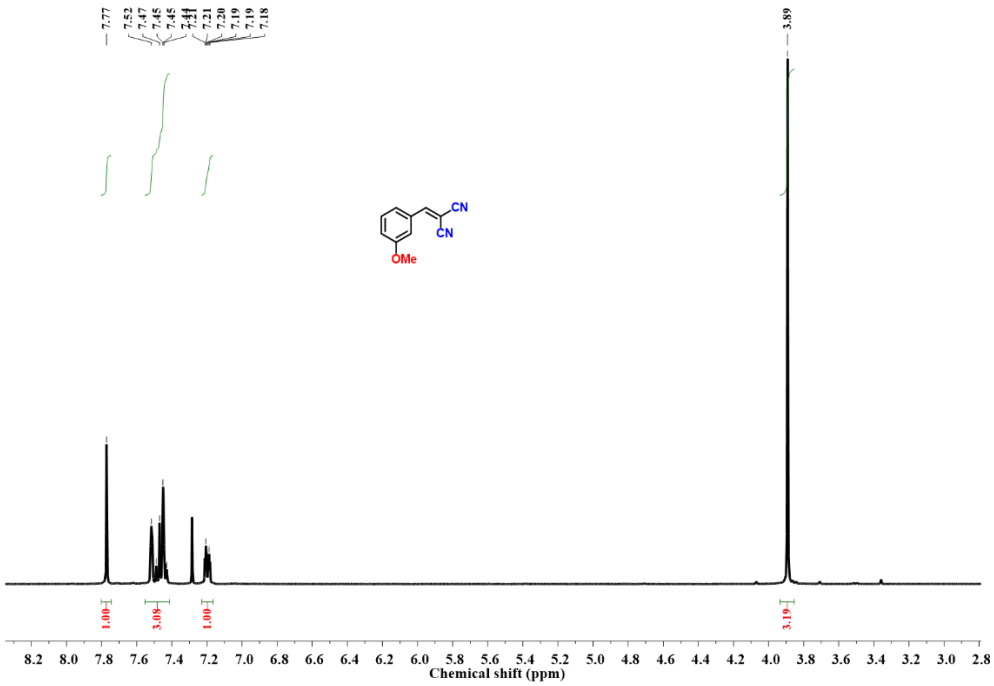

Figure S38. ^{1}H NMR spectrum of 2-(3-methoxybenzylidene)malononitrile (Table 1, entry 10) in $CDCl_3$.

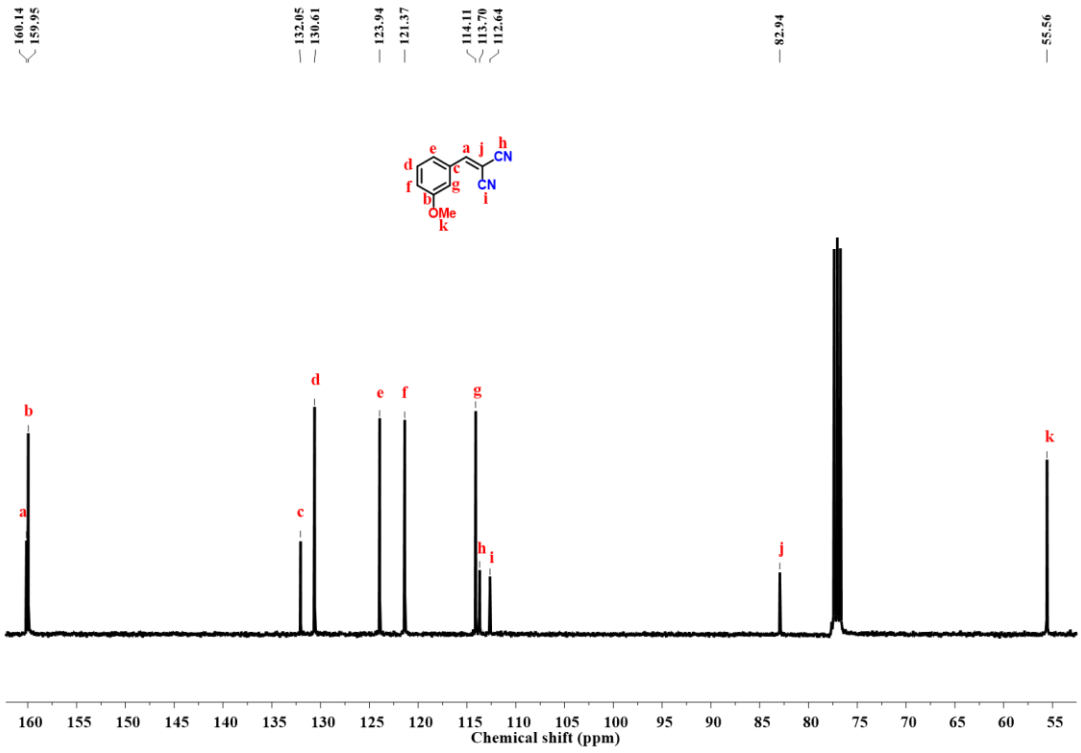

Figure S39. ^{13}C NMR spectrum of 2-(3-methoxybenzylidene)malononitrile (Table 1, entry 10) in $CDCl_3$.

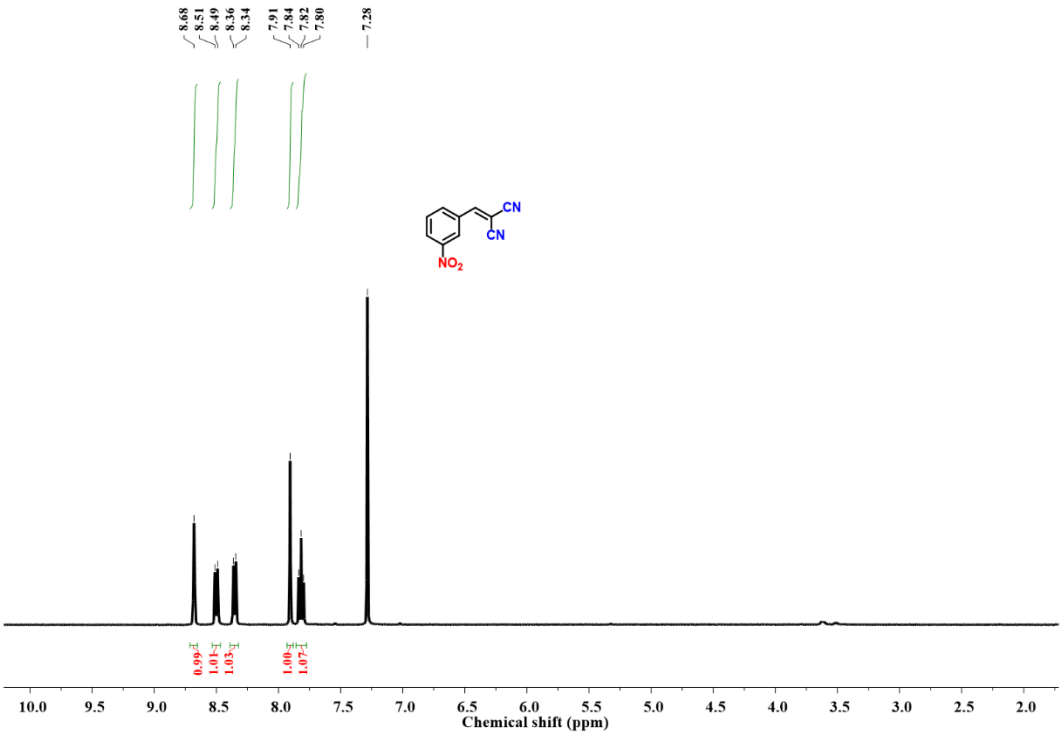

Figure S40. ^{1}H NMR spectrum of 2-(3-nitrobenzylidene)malononitrile (Table 1, entry 11) in $CDCl_3$.

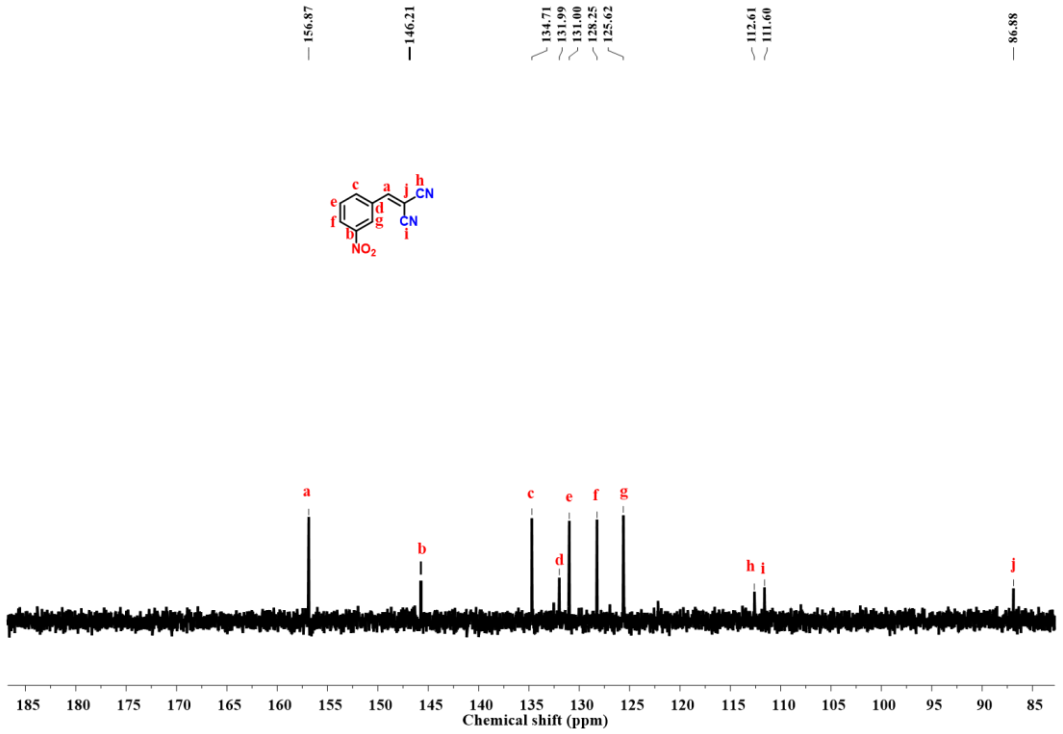

Figure S41. ^{13}C NMR spectrum of 2-(3-nitrobenzylidene)malononitrile (Table 1, entry 11) in $CDCl_3$.

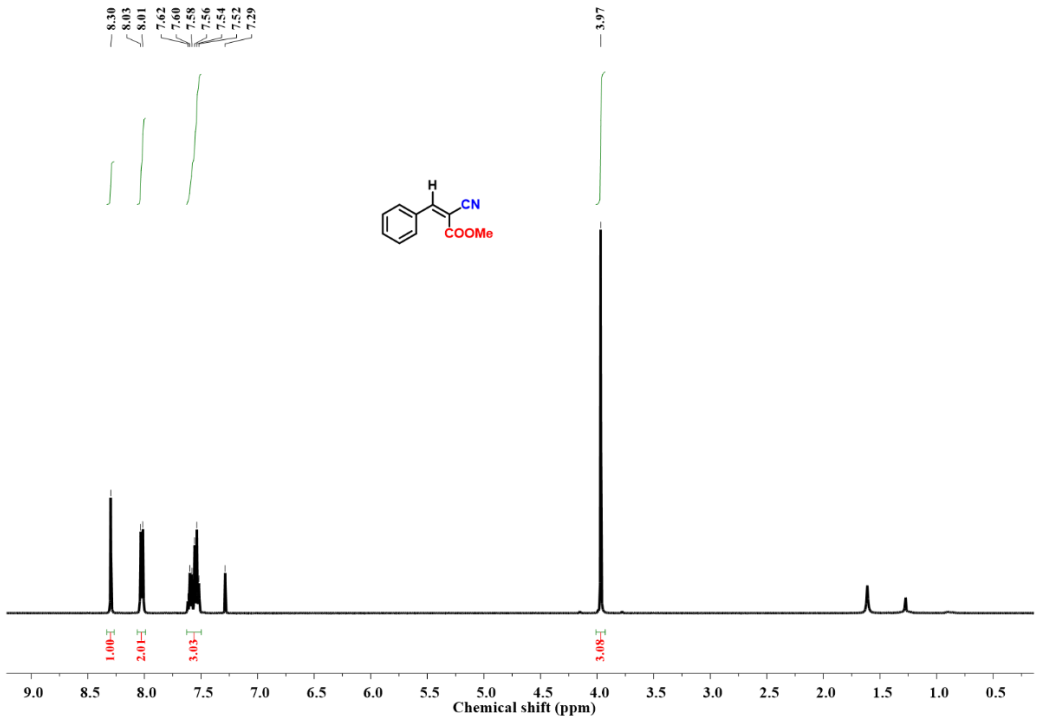

Figure S42. ^{1}H NMR spectrum of methyl 2-cyano-3-phenylacrylate (Table 1, entry 12) in $CDCl_3$.

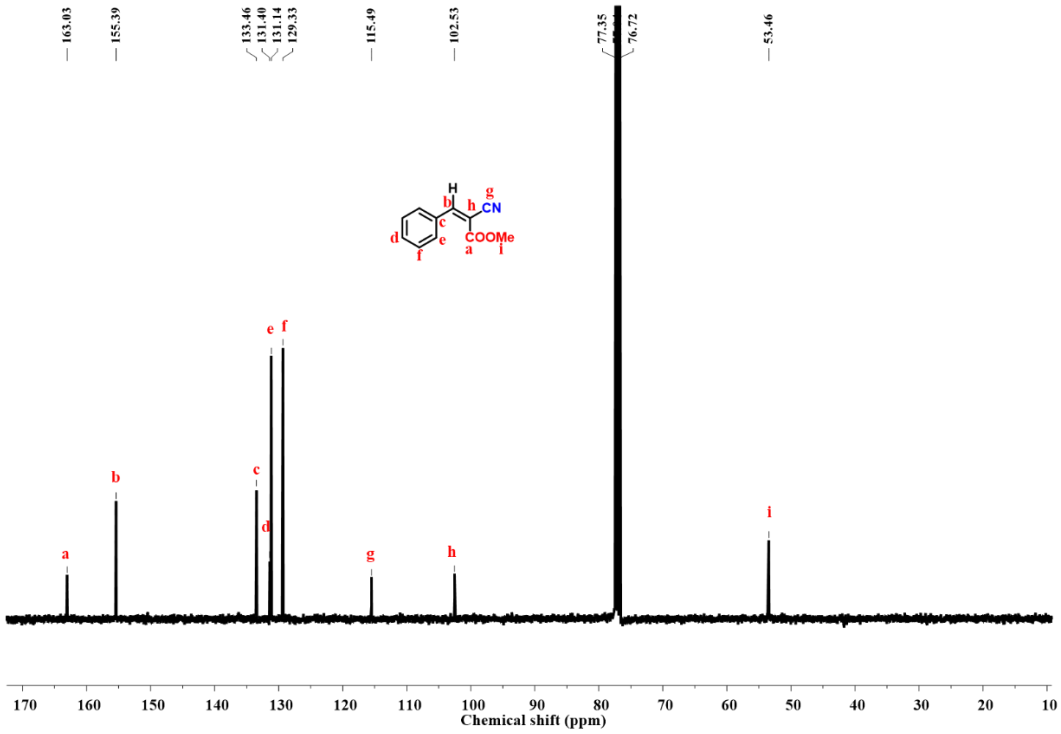

Figure S43. ^{13}C NMR spectrum of methyl 2-cyano-3-phenylacrylate (Table 1, entry 12) in $CDCl_3$.

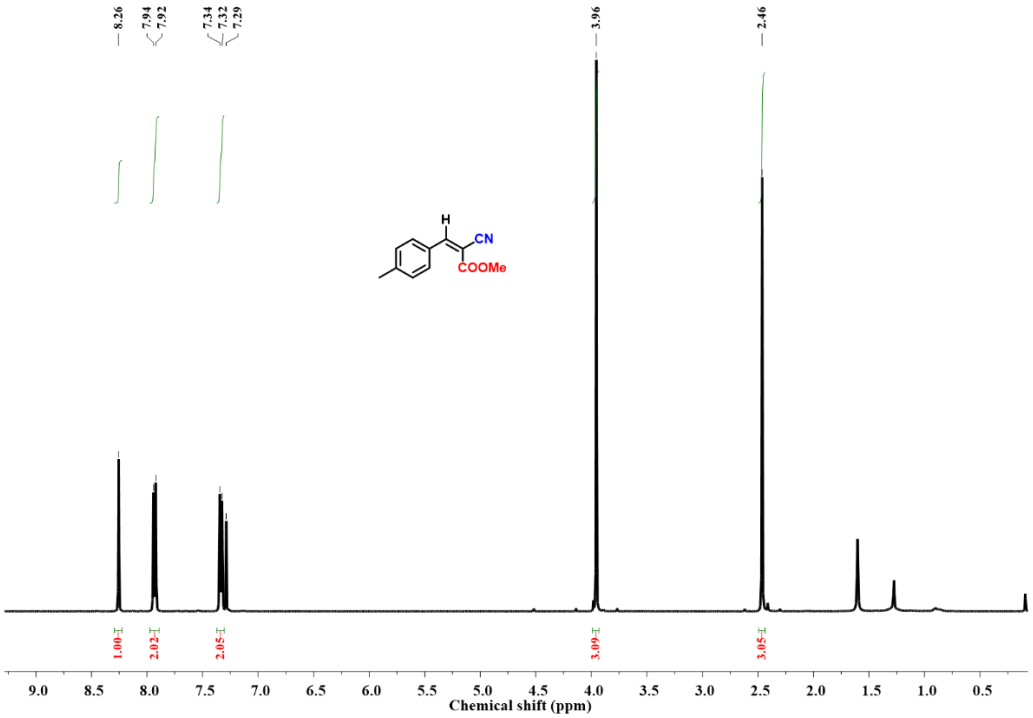

Figure S44. ^{1}H NMR spectrum of methyl 2-cyano-3-(*p*-tolyl)acrylate (Table 1, entry 13) in $CDCl_3$.

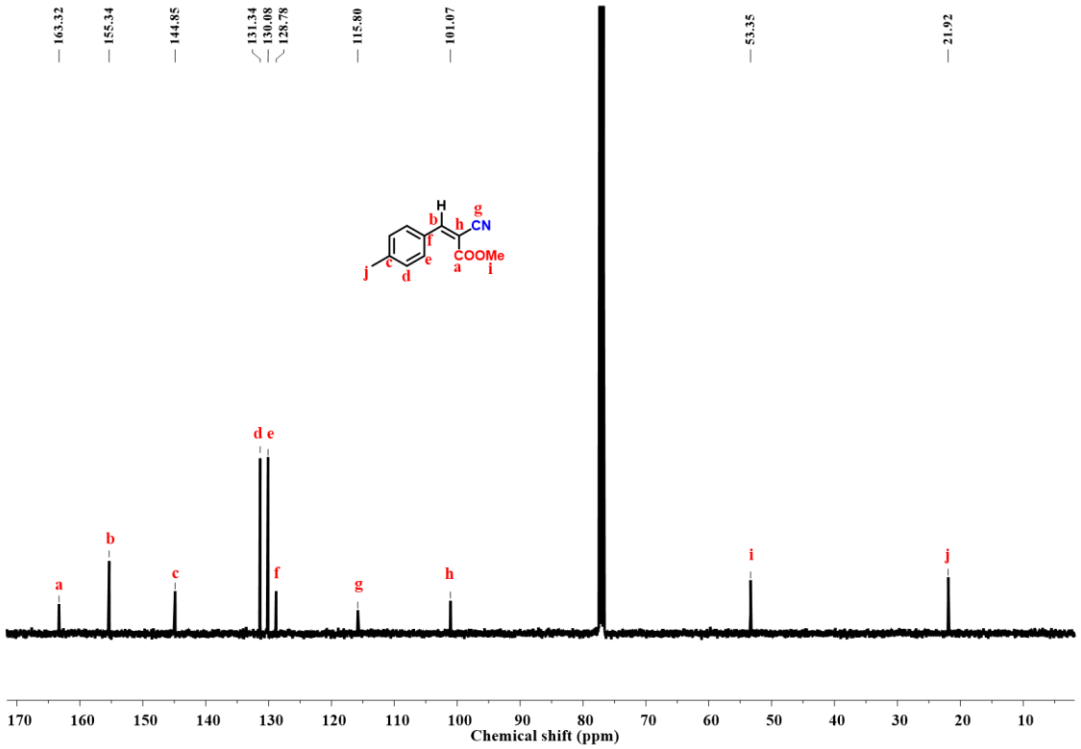

Figure S45. ^{13}C NMR spectrum of methyl 2-cyano-3-(*p*-tolyl)acrylate (Table 1, entry 13) in $CDCl_3$.

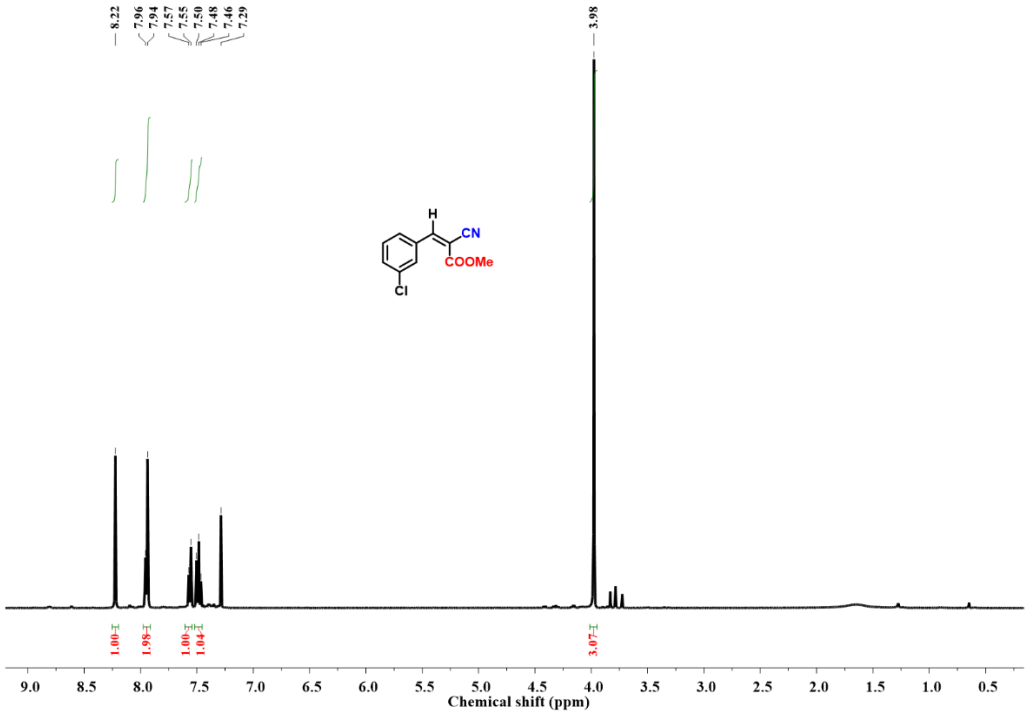

Figure S46. ^{1}H NMR spectrum of methyl 3-(3-chlorophenyl)-2-cyanoacrylate (Table 1, entry 14) in $CDCl_3$.

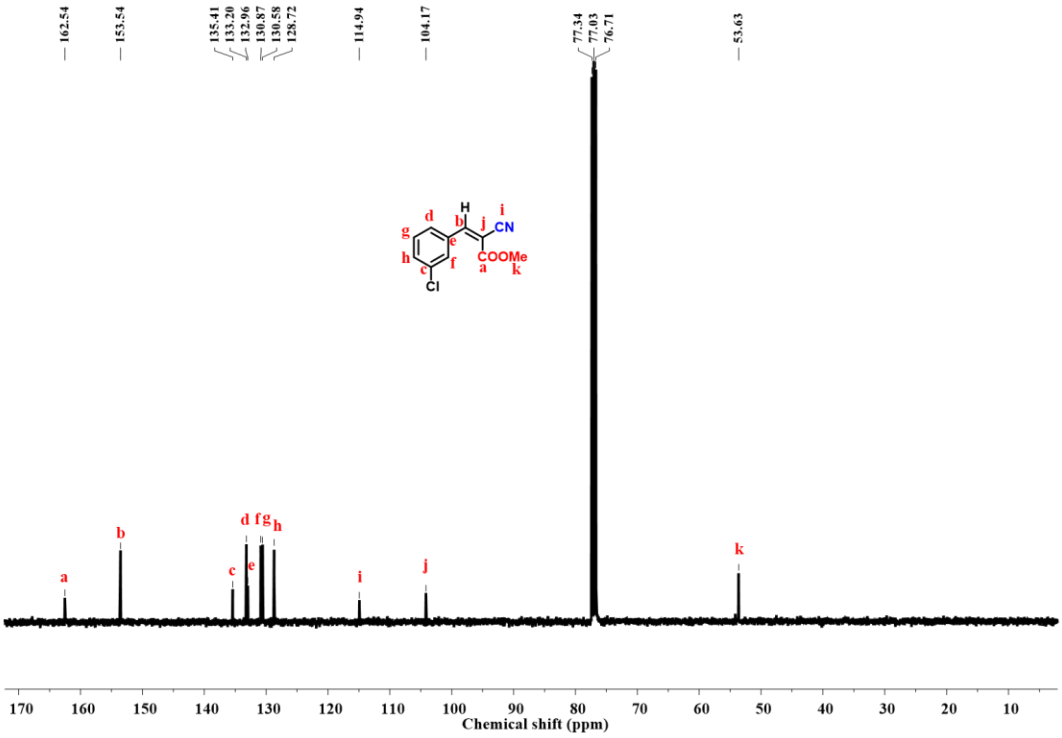

Figure S47. ^{13}C NMR spectrum of methyl 3-(3-chlorophenyl)-2-cyanoacrylate (Table 1, entry 14) in $CDCl_3$.

NMR spectra of the isolated products from the Strecker reaction:

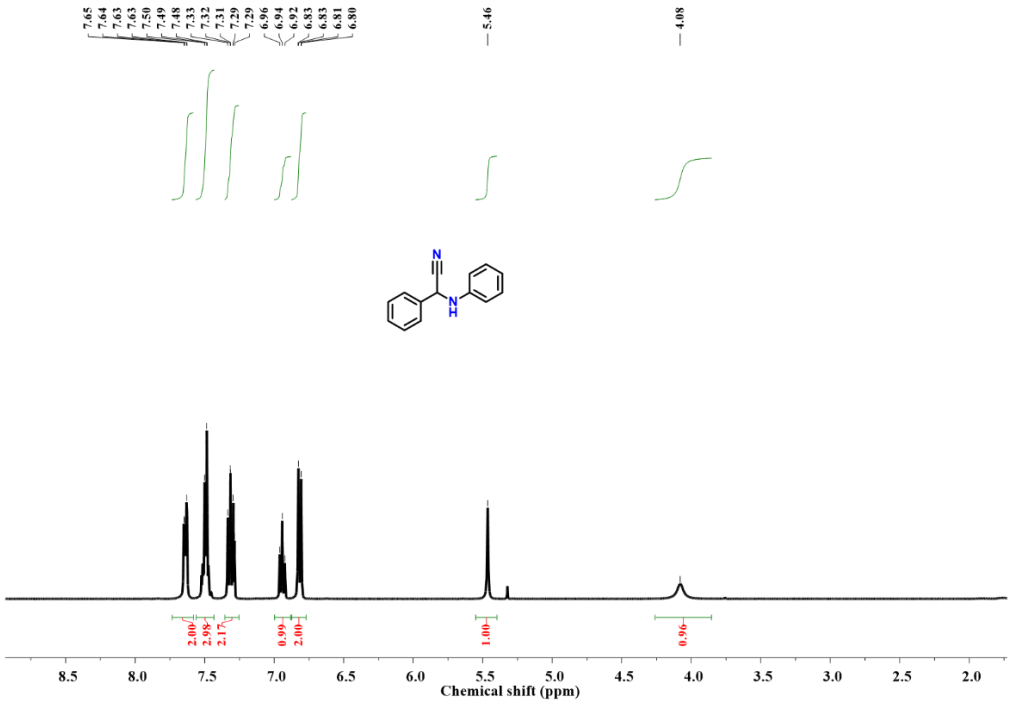

Figure S48. ^{1}H NMR spectrum of 2-phenyl-2-(phenylamino)acetonitrile (Table 2, entry 1) in $CDCl_3$.

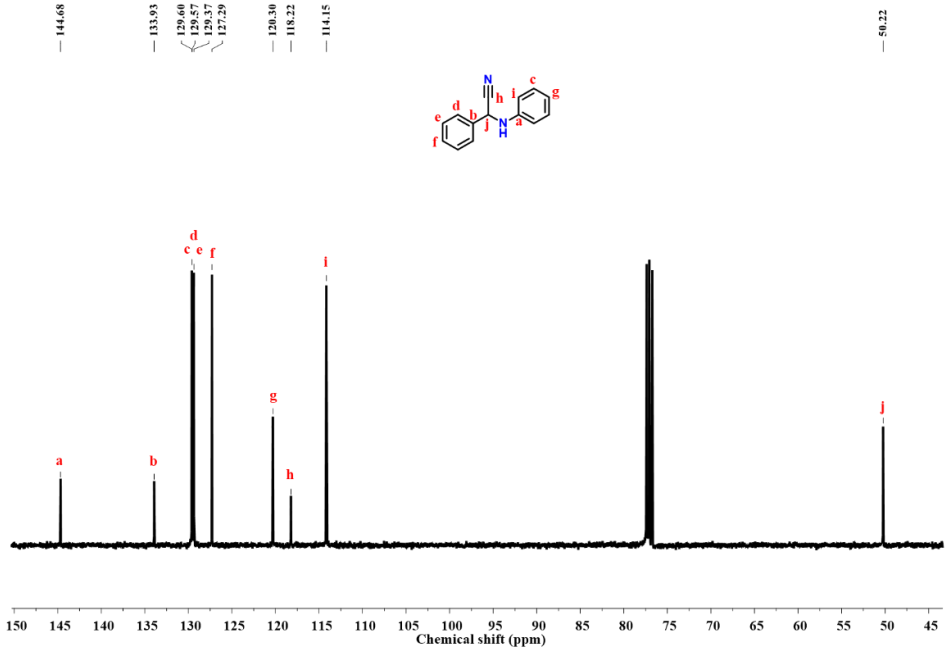

Figure S49. ^{13}C NMR spectrum of 2-phenyl-2-(phenylamino)acetonitrile (Table 2, entry 1) in $CDCl_3$.

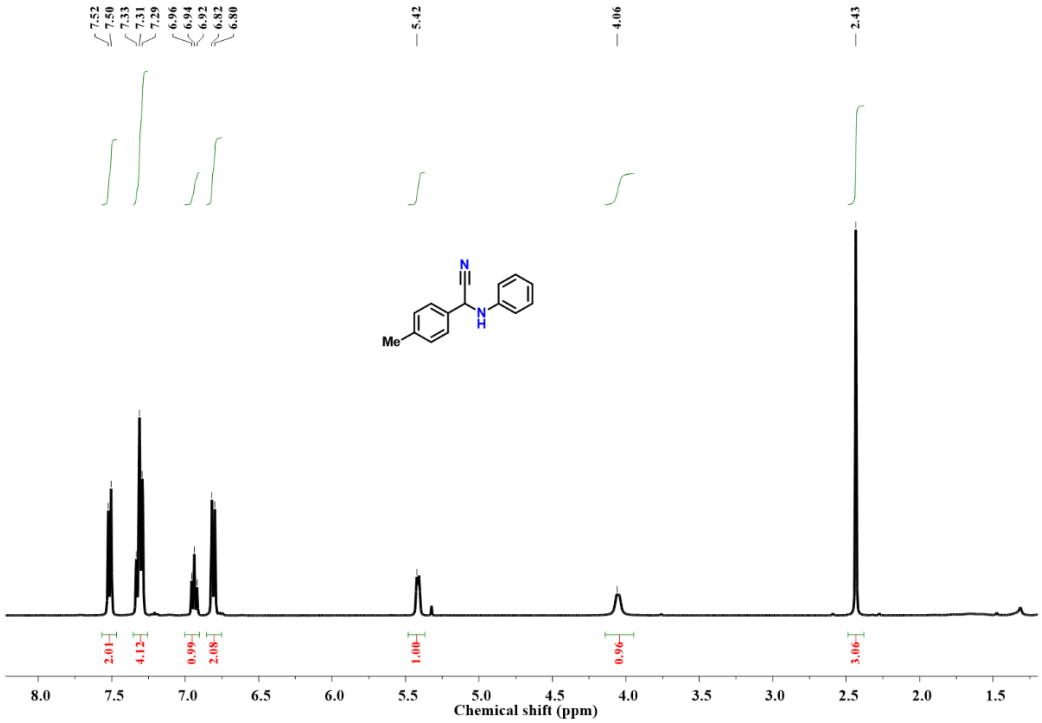

Figure S50. ^{1}H NMR spectrum of 2-(phenylamino)-2-(p-tolyl)acetonitrile (Table 2, entry 2) in $CDCl_3$.

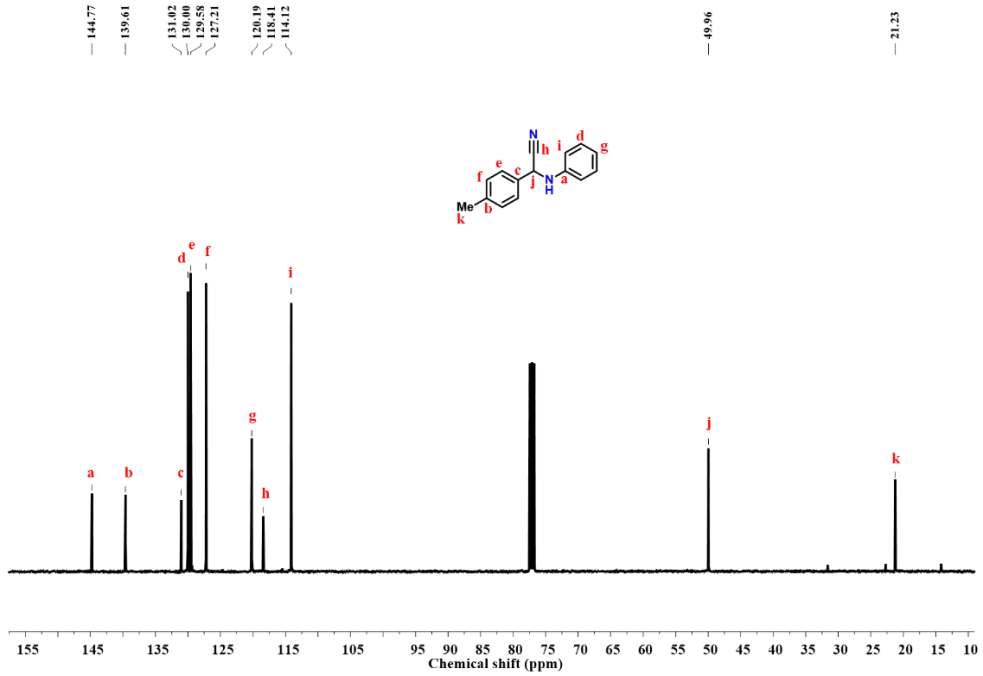

Figure S51. ^{13}C NMR spectrum of 2-(phenylamino)-2-(p-tolyl)acetonitrile (Table 2, entry 2) in $CDCl_3$.

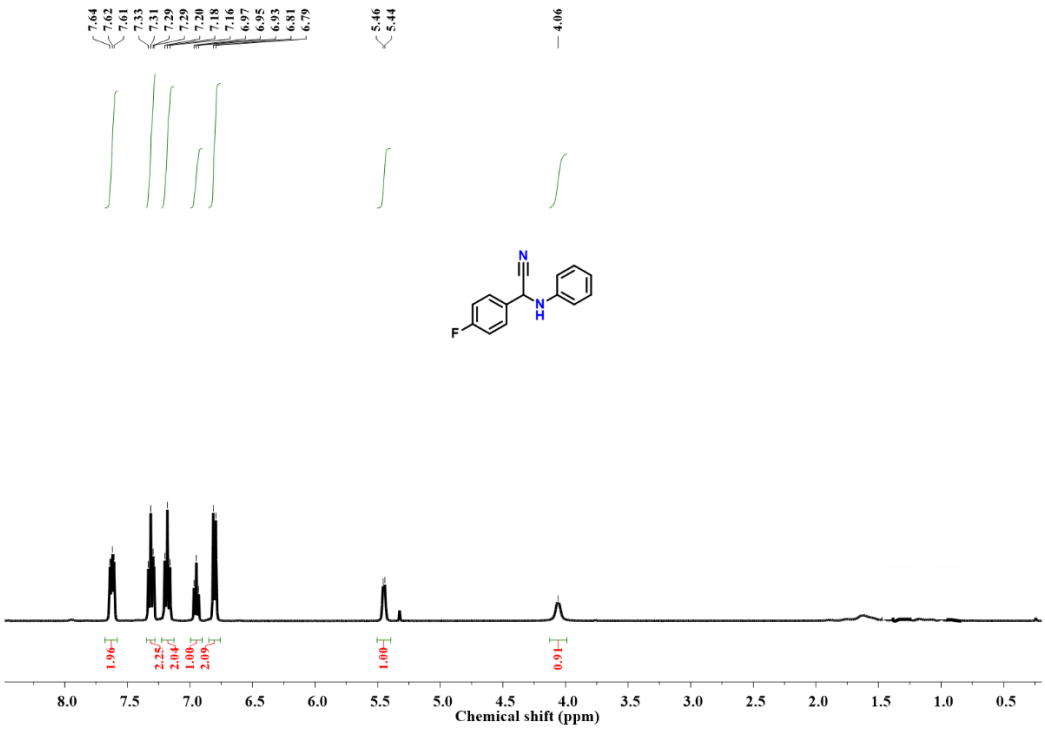

Figure S52. ^{1}H NMR spectrum of 2-(4-fluorophenyl)-2-(phenylamino)acetonitrile (Table 2, entry 3) in $CDCl_3$.

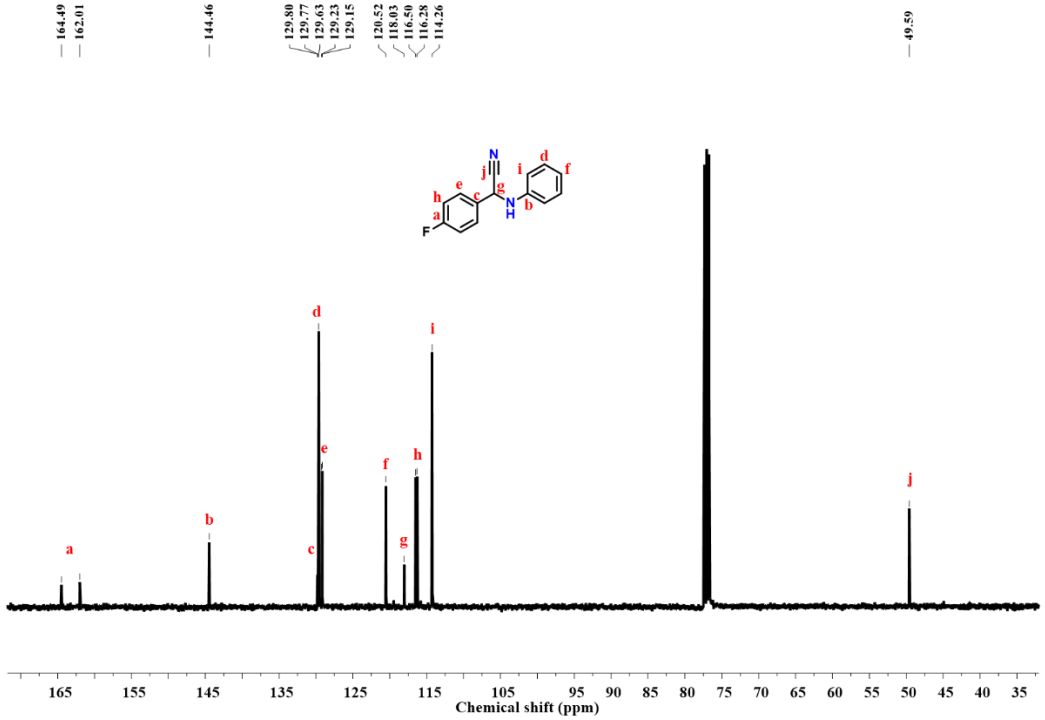

Figure S53. ^{13}C NMR spectrum of 2-(4-fluorophenyl)-2-(phenylamino)acetonitrile (Table 2, entry 3) in $CDCl_3$.

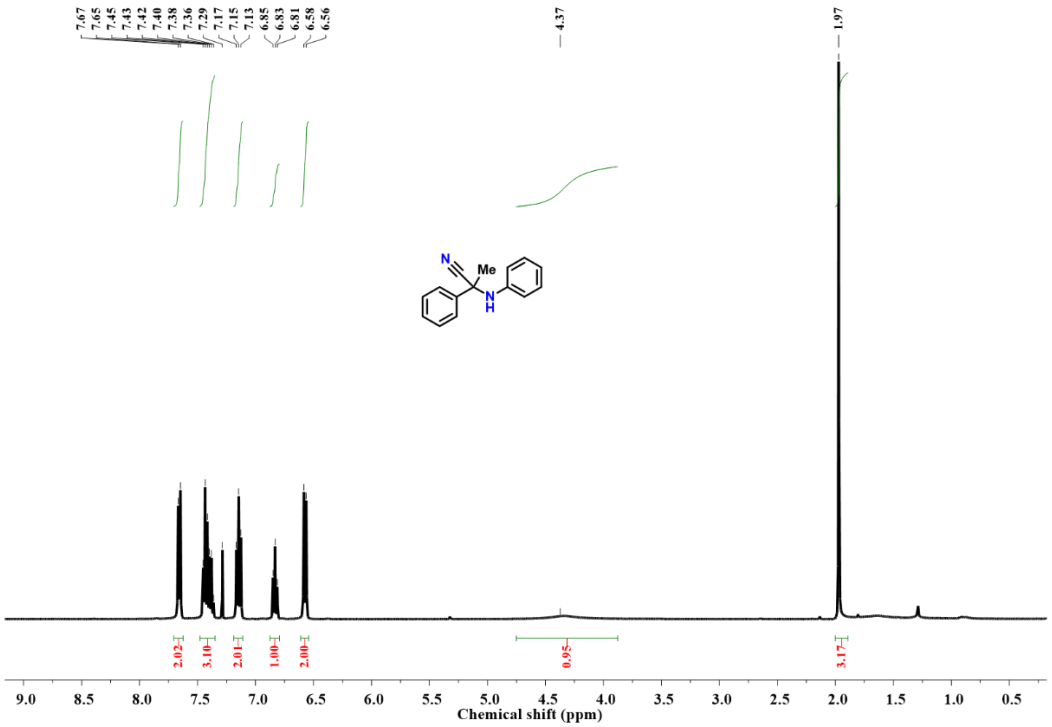

Figure S54. [1]H NMR spectrum of 2-phenyl-2-(phenylamino)propanenitrile (Table 2, entry 4) in $CDCl_3$.

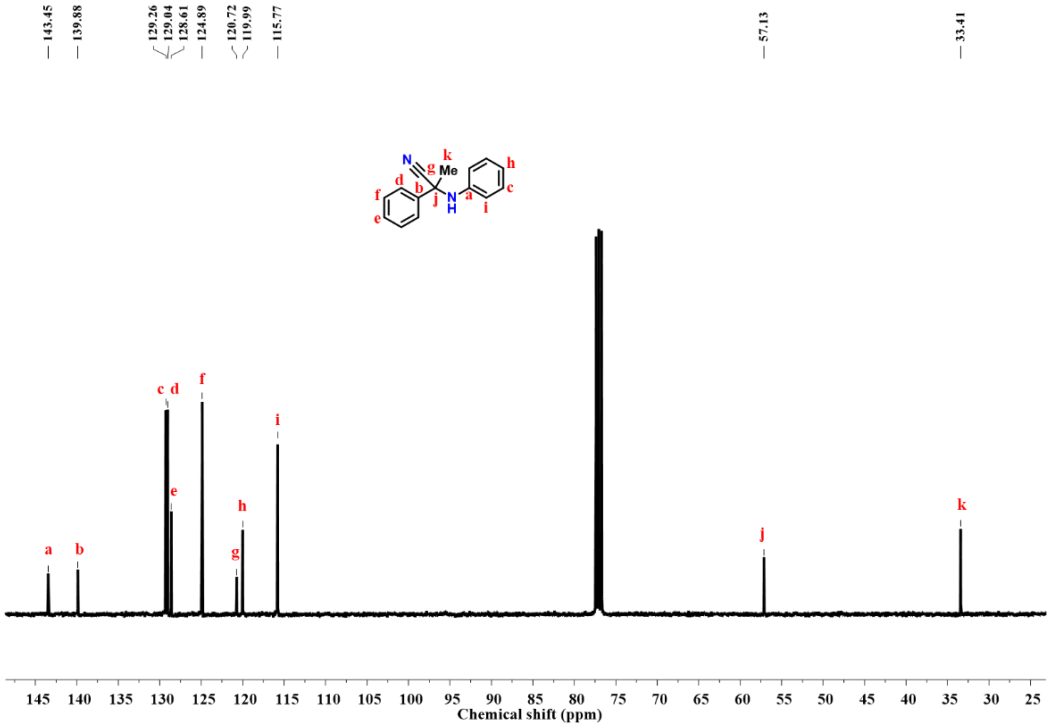

Figure S55. [13]C NMR spectrum of 2-phenyl-2-(phenylamino)propanenitrile (Table 2, entry 4) in $CDCl_3$.

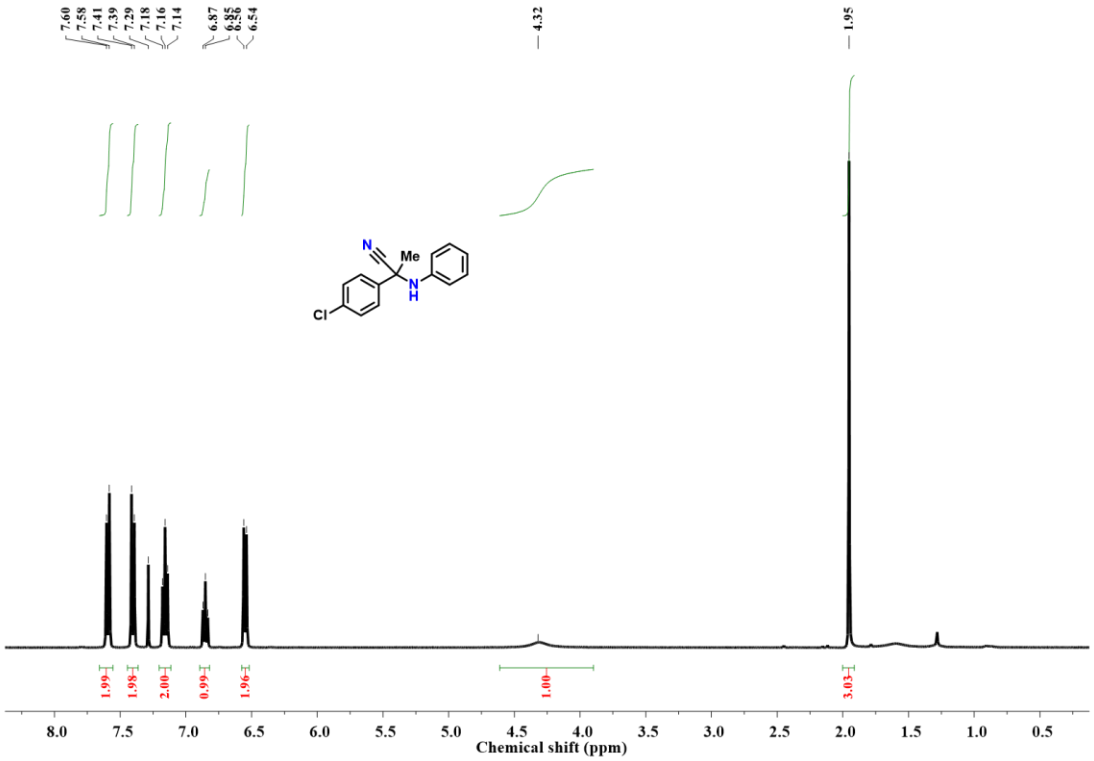

Figure S56. ^{1}H NMR spectrum of 2-(4-chlorophenyl)-2-(phenylamino)propanenitrile (Table 2, entry 5) in $CDCl_3$.

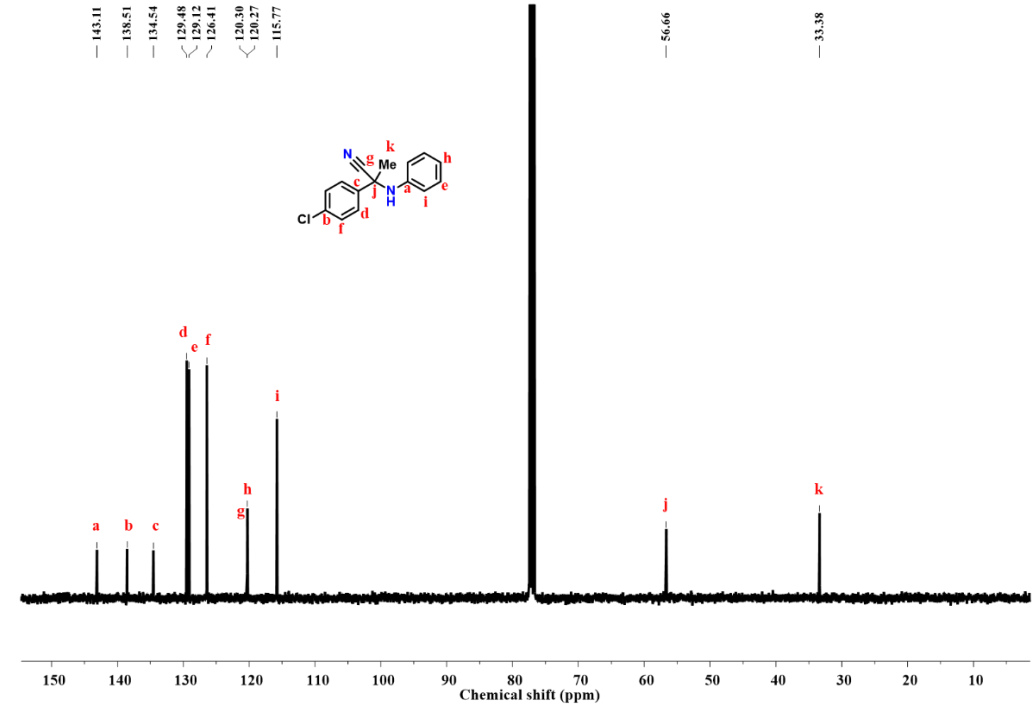

Figure S57. ^{13}C NMR spectrum of 2-(4-chlorophenyl)-2-(phenylamino)propanenitrile (Table 2, entry 5) in $CDCl_3$.

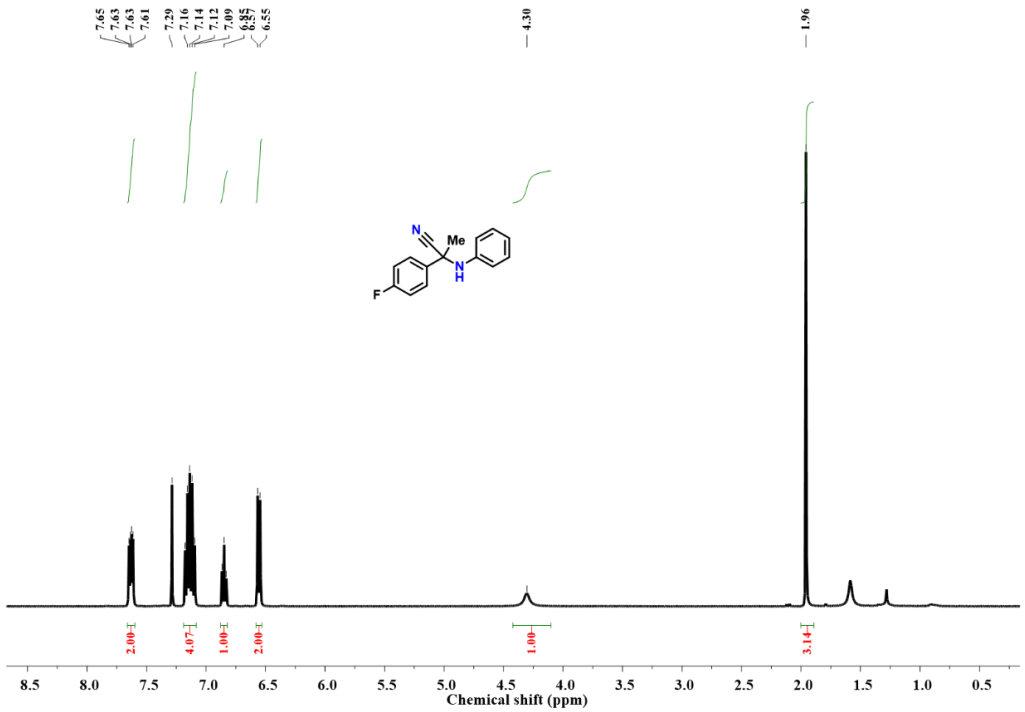

Figure S58. ^{1}H NMR spectrum of 2-(4-fluorophenyl)-2-(phenylamino)propanenitrile (Table 2, entry 6) in $CDCl_3$.

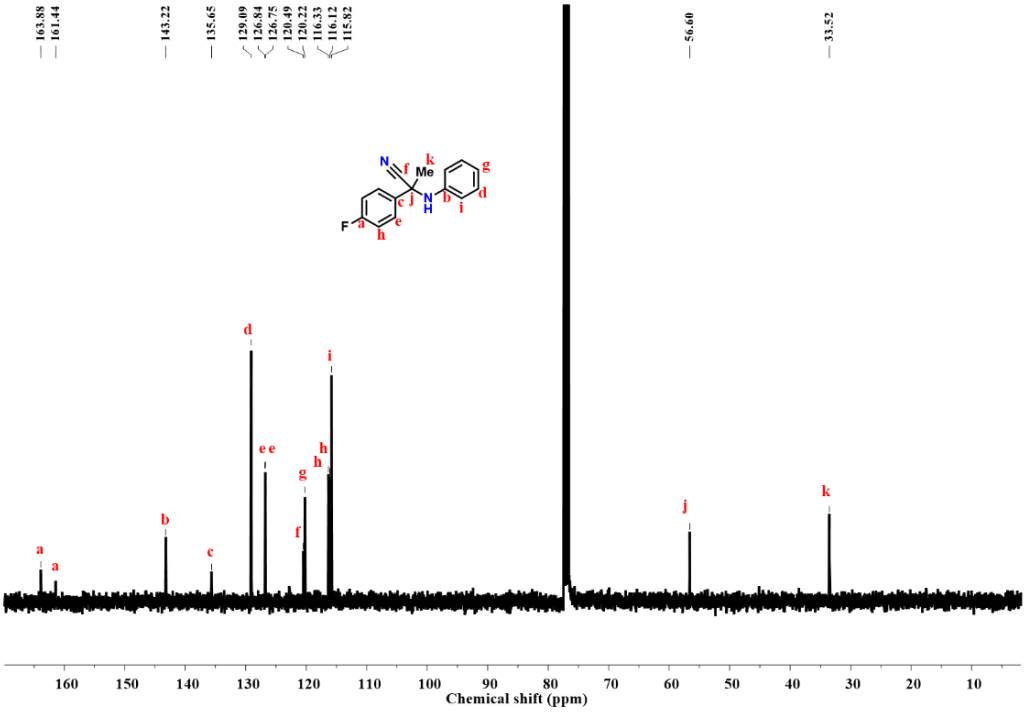

Figure S59. ^{13}C NMR spectrum of 2-(4-fluorophenyl)-2-(phenylamino)propanenitrile (Table 2, entry 6) in $CDCl_3$.

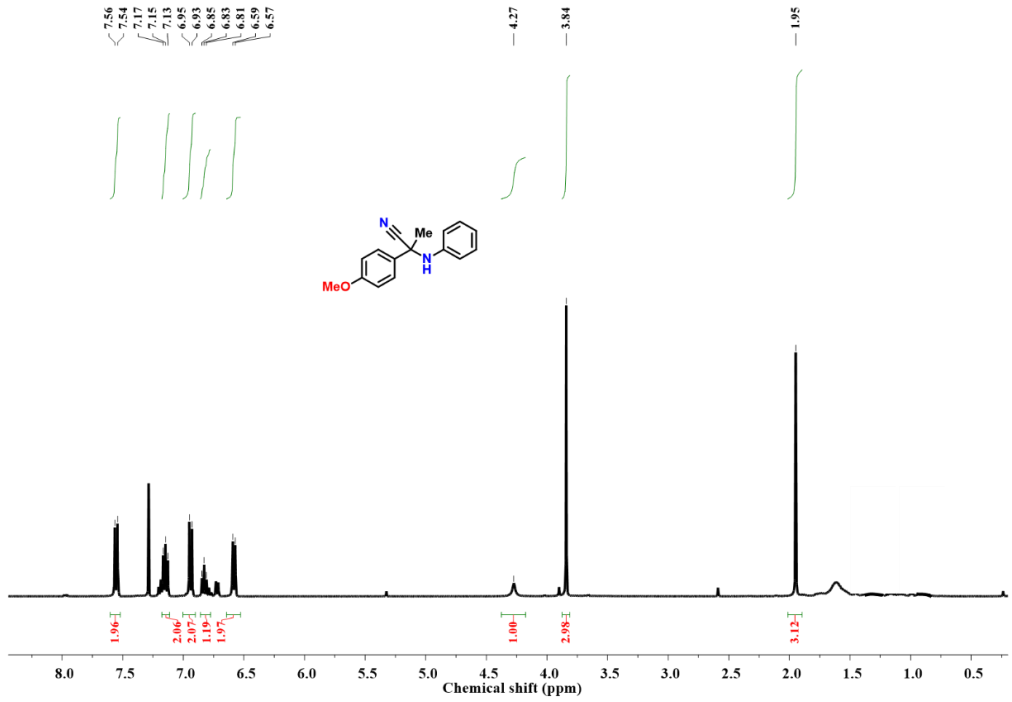

Figure S60. ^{1}H NMR spectrum of 2-(4-methoxyphenyl)-2-(phenylamino)propanenitrile (Table 2, entry 7) in $CDCl_3$.

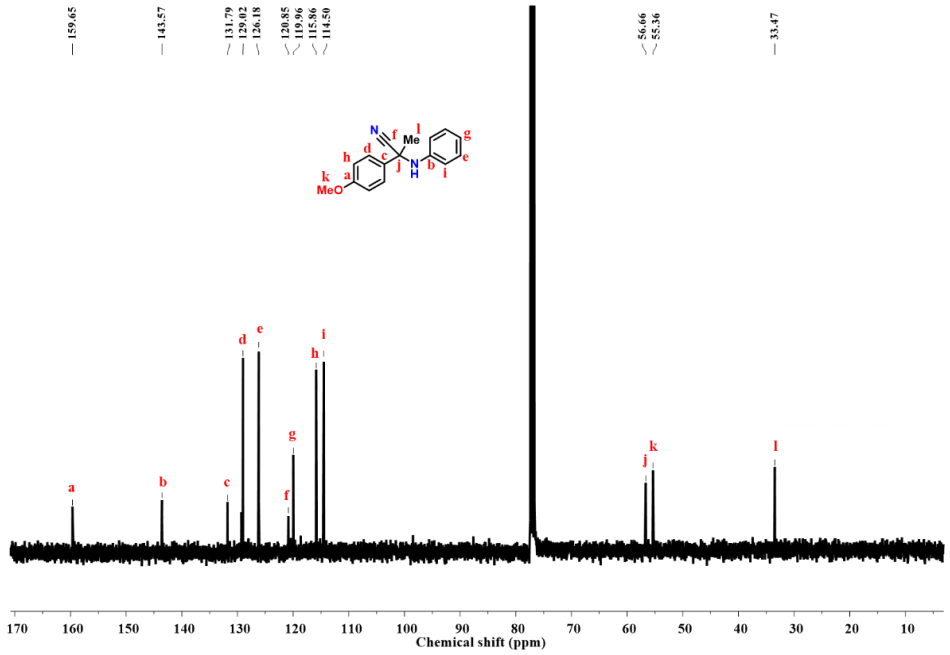

Figure S61. ^{13}C NMR spectrum of 2-(4-methoxyphenyl)-2-(phenylamino)propanenitrile (Table 2, entry 7) in $CDCl_3$.

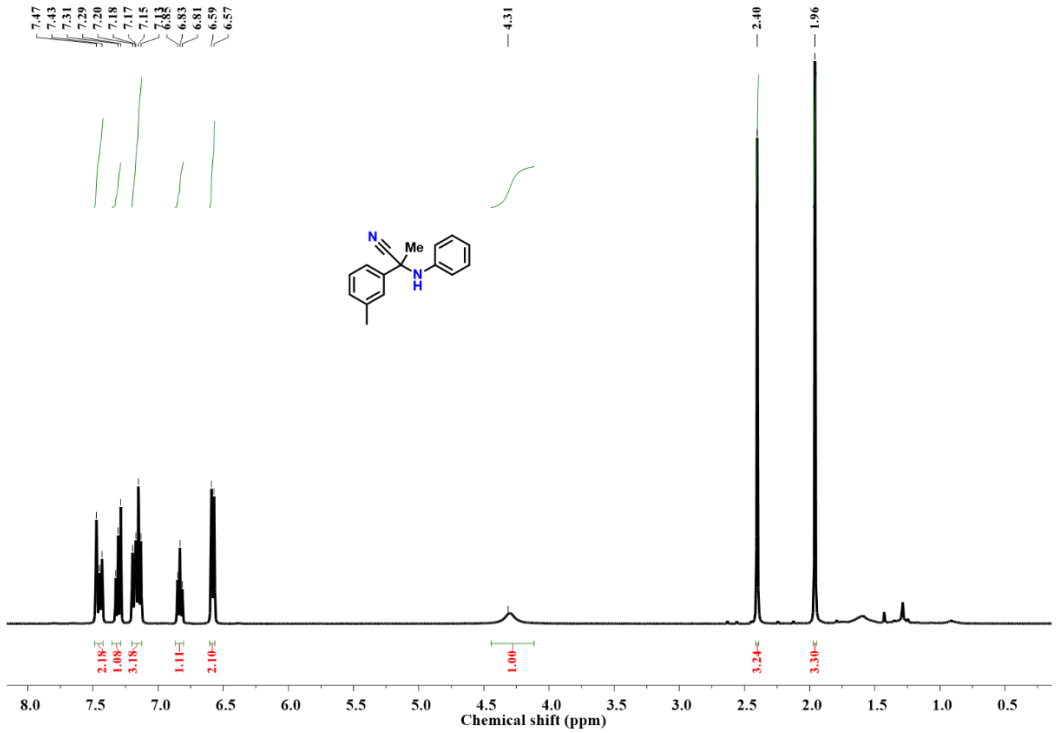

Figure S62. ^{1}H NMR spectrum of 2-(phenylamino)-2-(m-tolyl)propanenitrile (Table 2, entry 8) in $CDCl_3$.

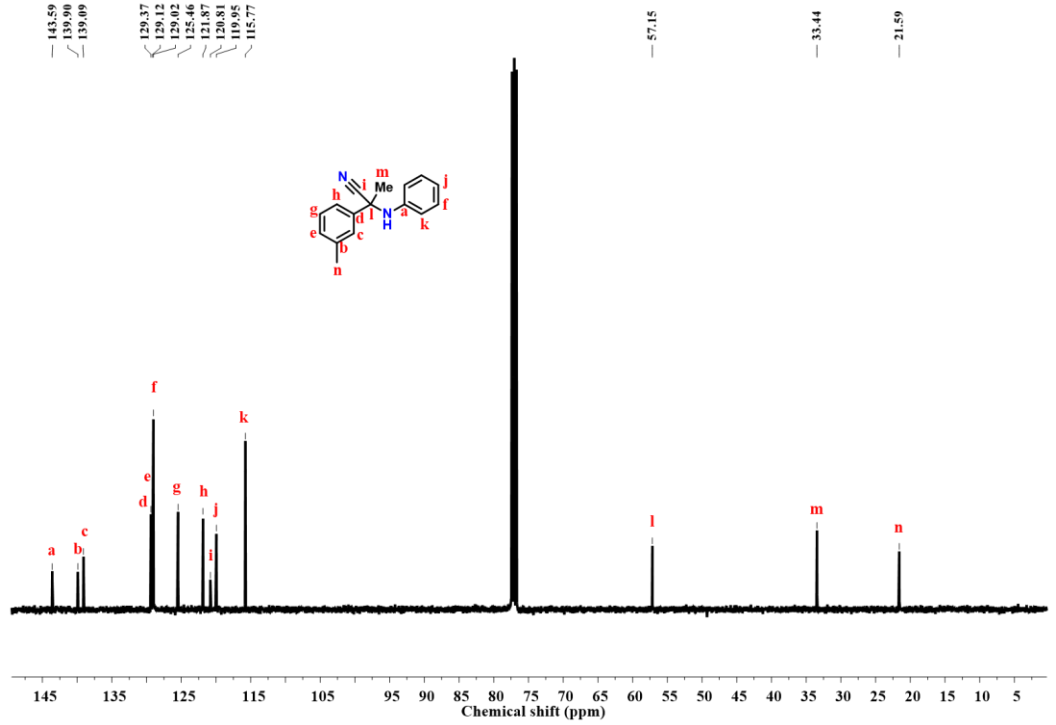

Figure S63. ^{13}C NMR spectrum of 2-(phenylamino)-2-(m-tolyl)propanenitrile (Table 2, entry 8) in $CDCl_3$.

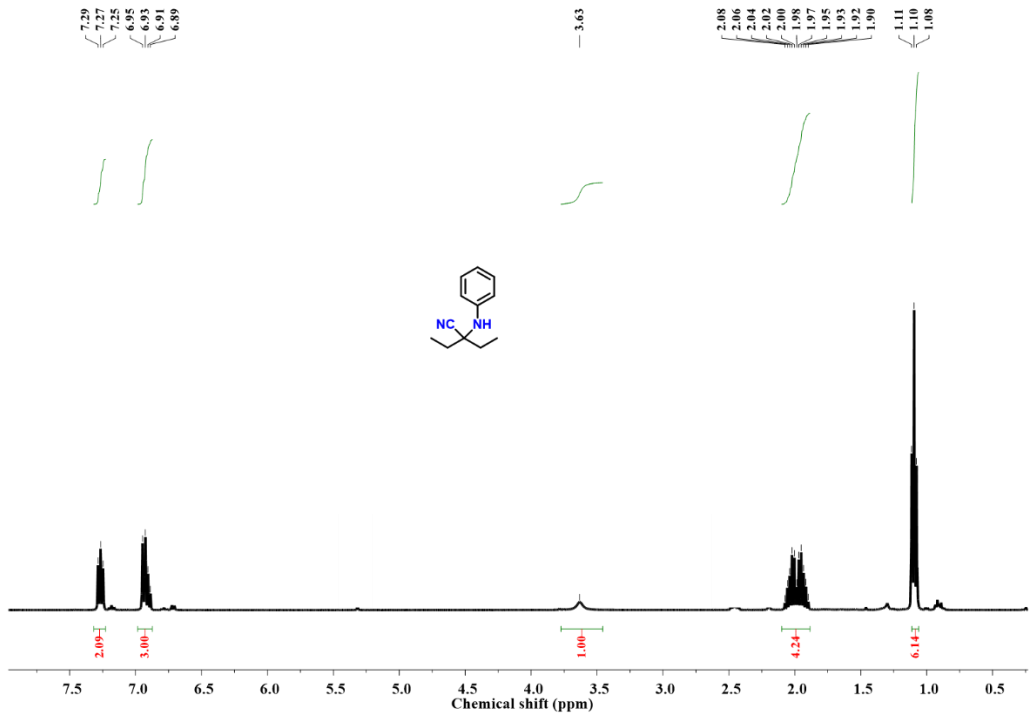

Figure S64. ^{1}H NMR spectrum of 2-ethyl-2-(phenylamino)butanenitrile (Table 2, entry 9) in $CDCl_3$.

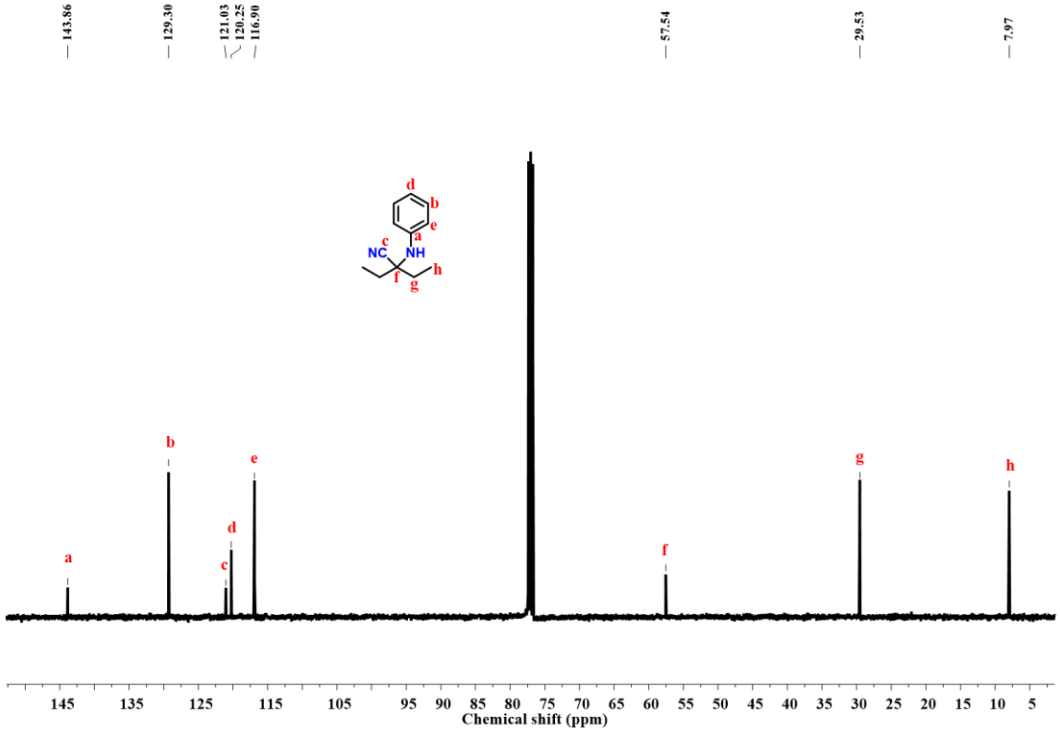

Figure S65. ^{13}C NMR spectrum of 2-ethyl-2-(phenylamino)butanenitrile (Table 2, entry 9) in $CDCl_3$.

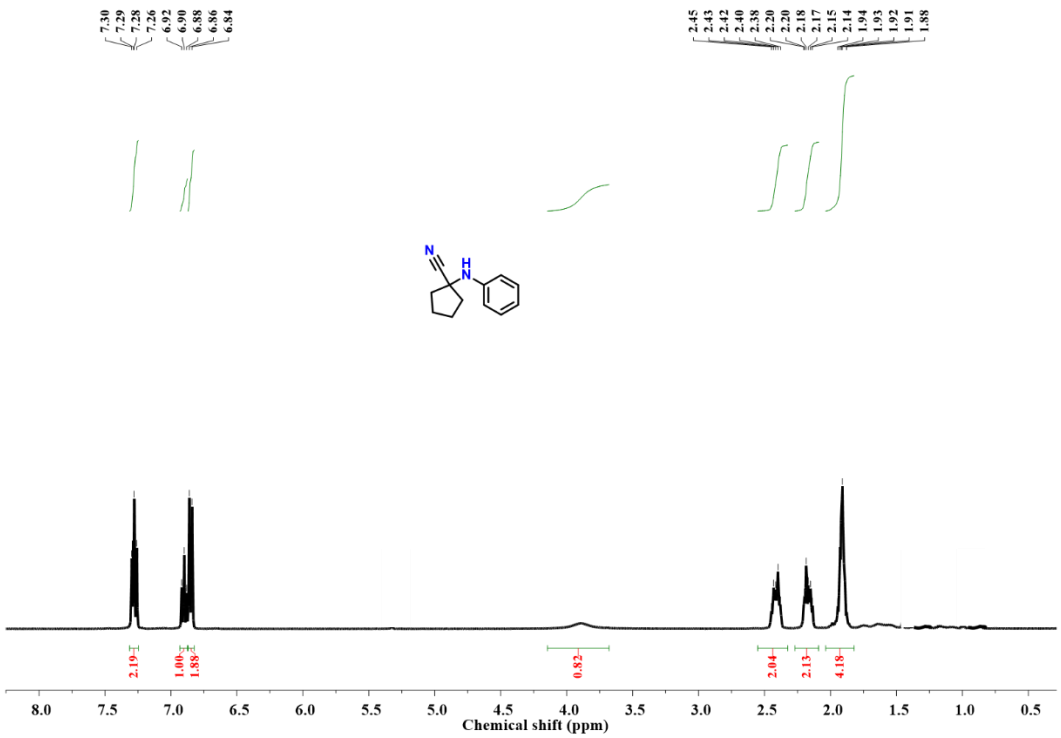

Figure S66. ^{1}H NMR spectrum of 1-(phenylamino)cyclopentanecarbonitrile (Table 2, entry 10) in $CDCl_3$.

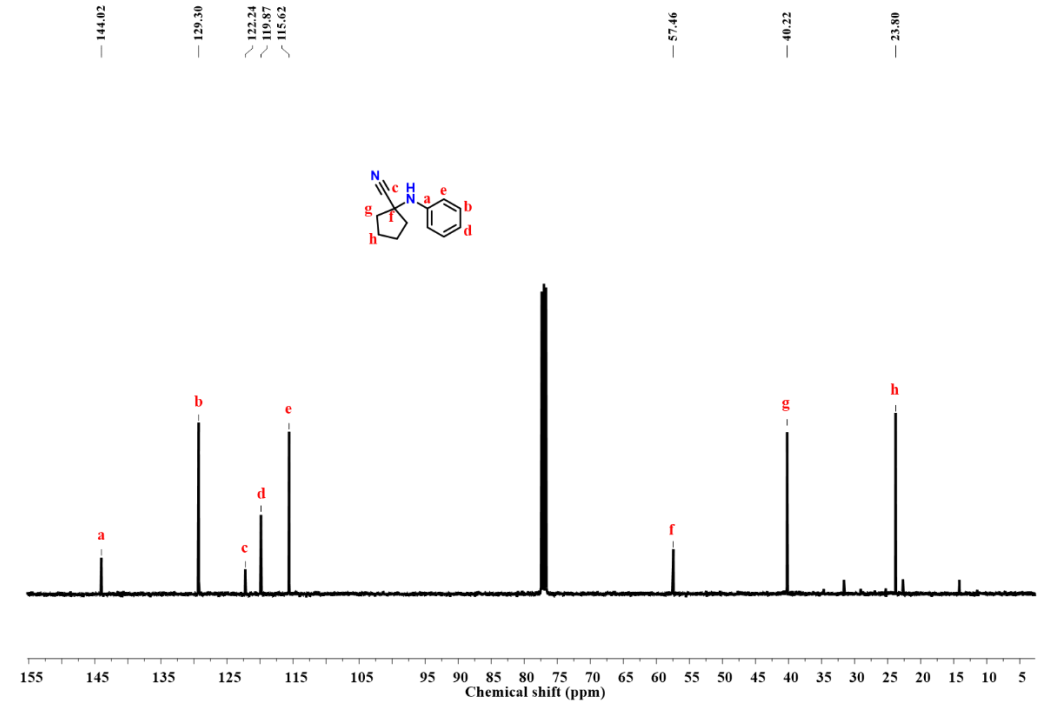

Figure S67. ^{13}C NMR spectrum of 1-(phenylamino)cyclopentanecarbonitrile (Table 2, entry 10) in $CDCl_3$.

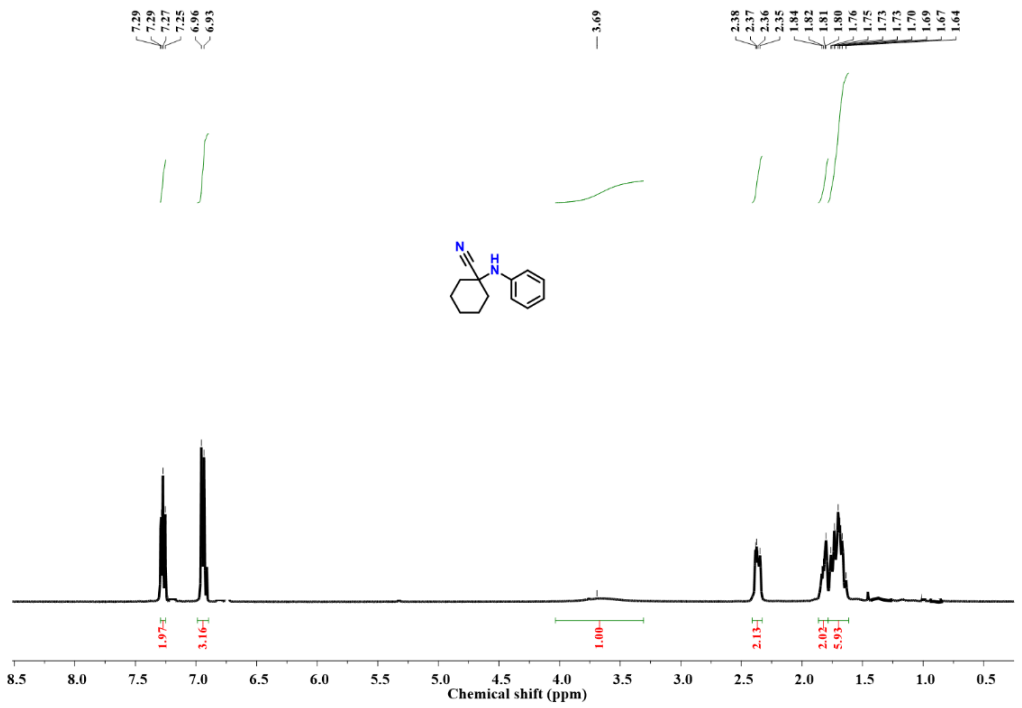

Figure S68. ^{1}H NMR spectrum of 1-(phenylamino)cyclohexanecarbonitrile (Table 2, entry 11) in $CDCl_3$.

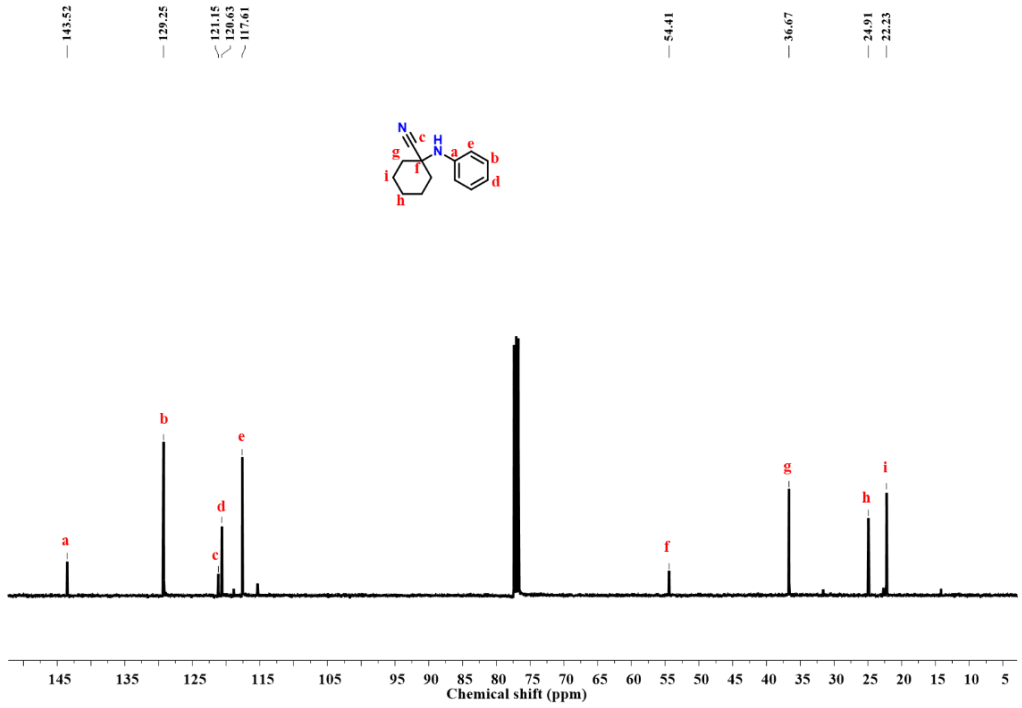

Figure S69. ^{13}C NMR spectrum of 1-(phenylamino)cyclohexanecarbonitrile (Table 2, entry 11) in $CDCl_3$.

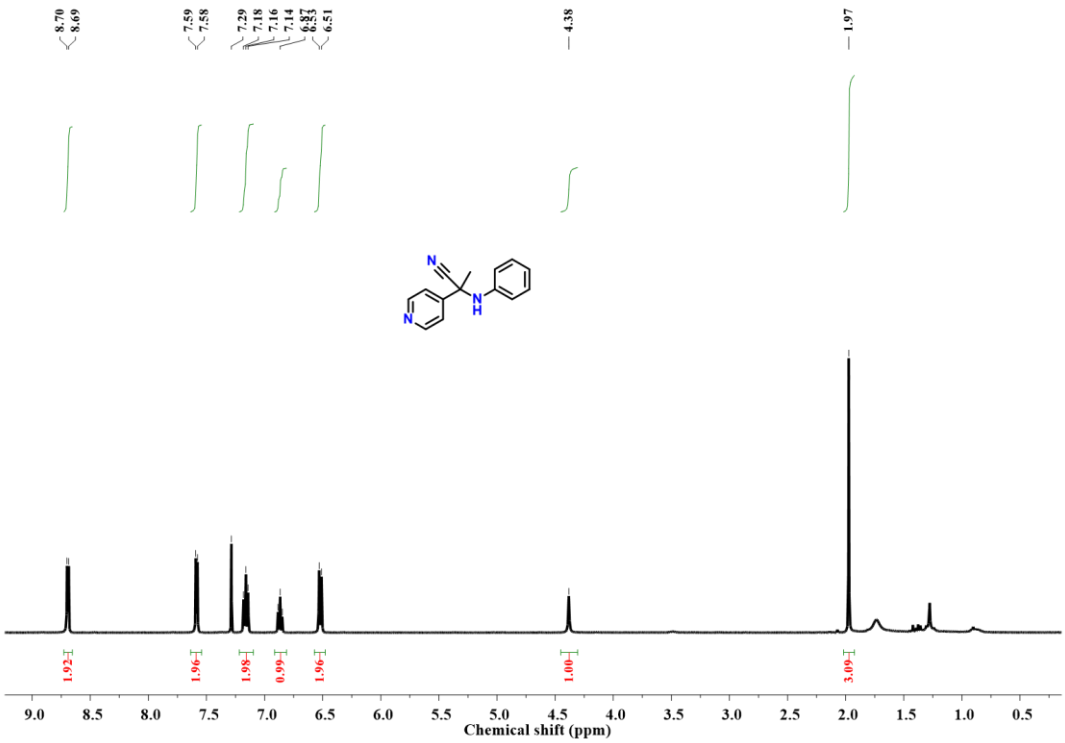

Figure S70. ^{1}H NMR spectrum of 2-(phenylamino)-2-(pyridin-4-yl)propanenitrile (Table 2, entry 12) in $CDCl_3$.

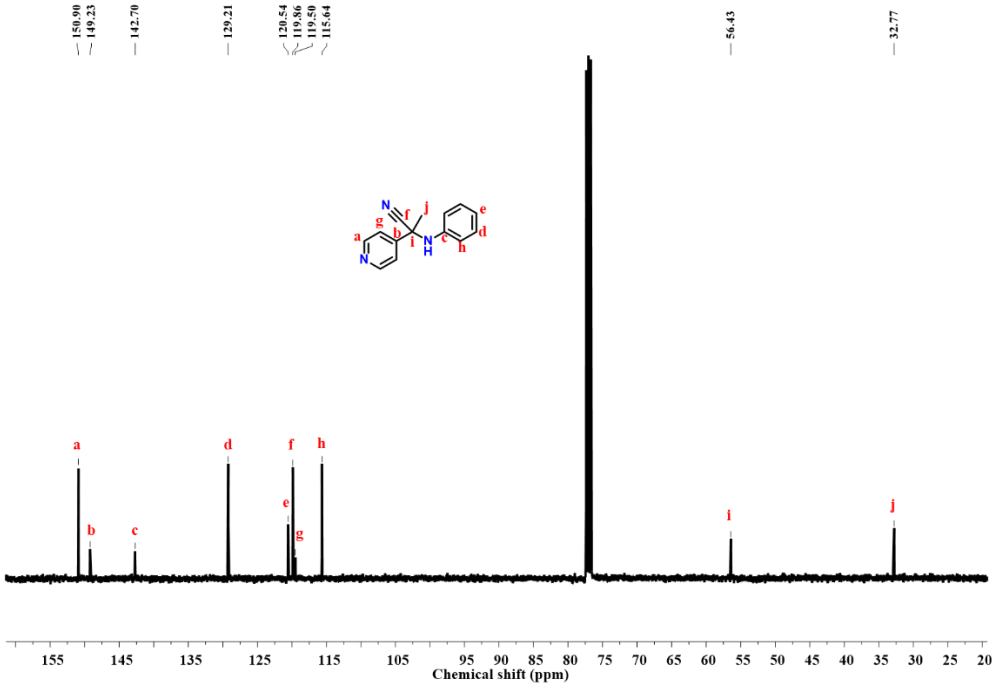

Figure S71. ^{13}C NMR spectrum of 2-(phenylamino)-2-(pyridin-4-yl)propanenitrile (Table 2, entry 12) in $CDCl_3$.

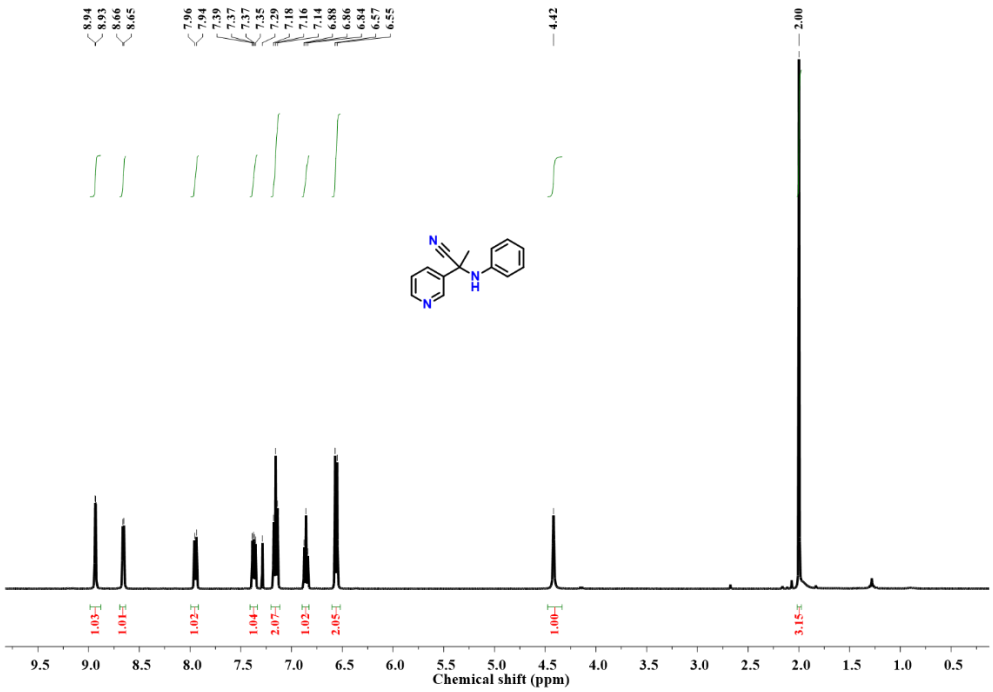

Figure S72. ^{1}H NMR spectrum of 2-(phenylamino)-2-(pyridin-3-yl)propanenitrile (Table 2, entry 13) in $CDCl_3$.

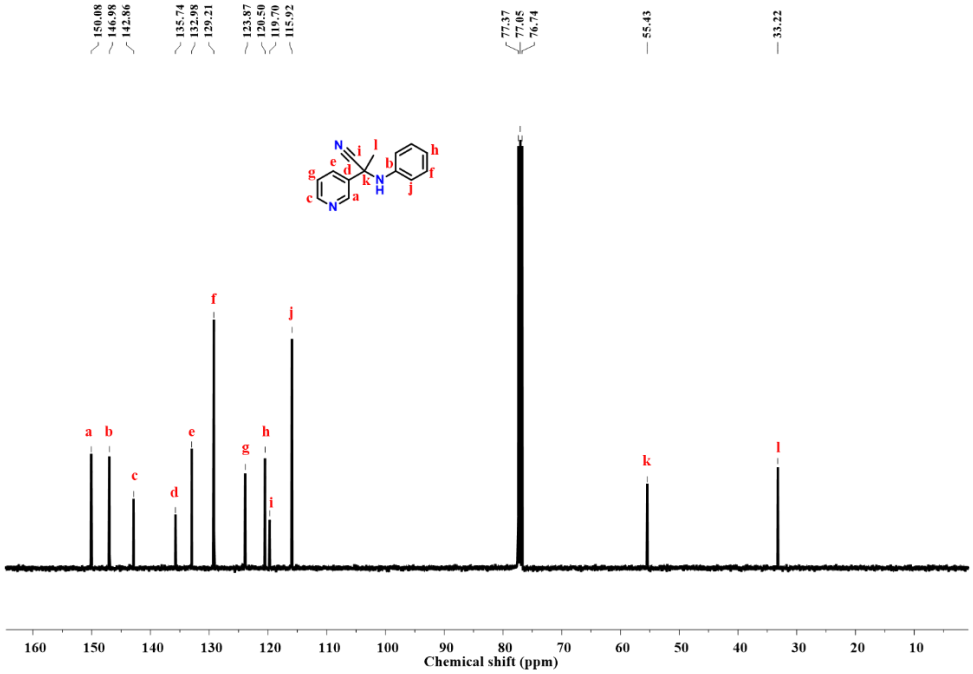

Figure S73. ^{13}C NMR spectrum of 2-(phenylamino)-2-(pyridin-3-yl)propanenitrile (Table 2, entry 13) in $CDCl_3$.

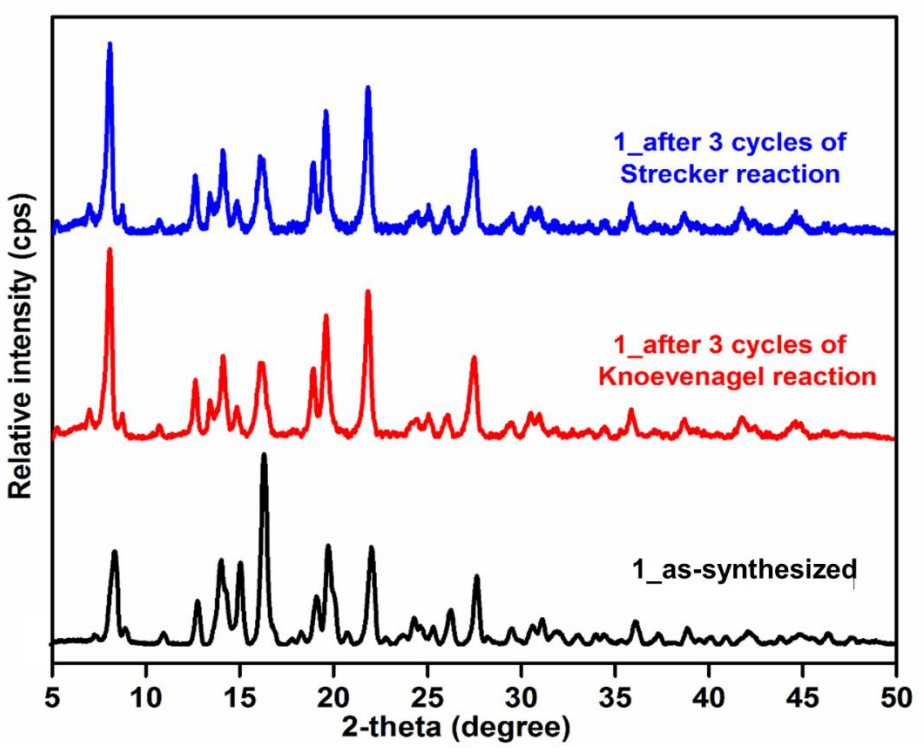

Figure S74. PXRD patterns of **1** before and after catalysis experiments.

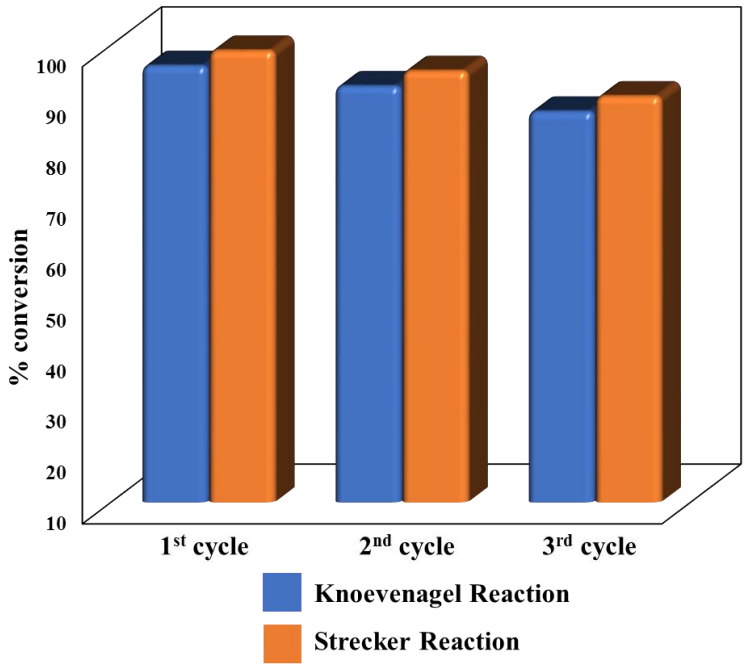

Figure S75. % conversion for three consecutive cycles of (i) Knoevenagel condensation reaction of benzaldehyde and malononitrile and (ii) Strecker reaction of benzaldehyde with aniline and trimethylsilyl cyanide, catalysed by **1**.

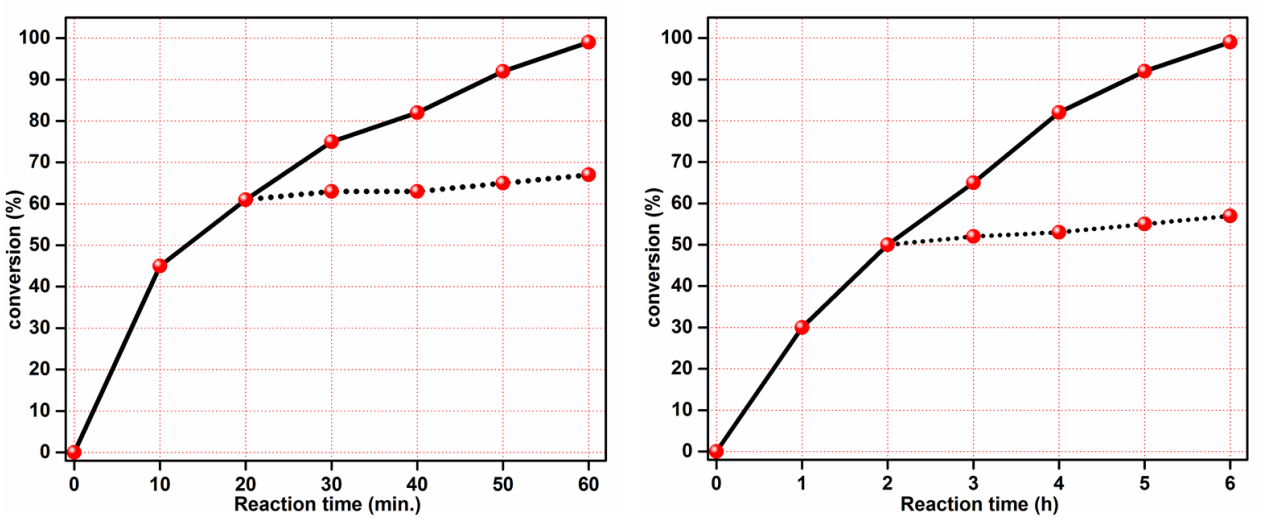

Figure S76. Progress of the reaction with time in presence of catalyst **1** (solid lines) and after separating the catalyst from the reaction mixture (dotted lines) for: (left) Knoevenagel reaction of benzaldehyde with malononitrile, and (right) Strecker reaction of benzaldehyde with aniline and trimethylsilyl cyanide.

Single Crystal X-ray Data Collection and Refinement. Using an optical microscope, one suitable crystal of 1 was put inside a nylon loop attached to a goniometer head which was then placed under a cold stream of nitrogen gas for slow cooling to 100 K. Based on the crystal suitability from diffraction photographs and unit cell determination, data were collected on a Kappa APEX II diffractometer as described earlier from our laboratory.[S1] After integration of the data by the program SAINT[S2] to obtain values of F^2 and $\sigma(F^2)$ for each reflection, data were further corrected for Lorentz and polarization effects followed by the application of an absorption correction (SADABS).[S2] The crystal structure was solved by direct method using SHELXS program of SHELXTL package and refined by full-matrix least square methods with SHELXL-2014[S3] within the OLEX2 crystallographic software suite.[S4] The space group was chosen based on systematic absences and confirmed by the successful refinement of the structure. Several full-matrix least-squares/difference Fourier cycles were performed to complete the refinement of the structure to convergence. All non-hydrogen atoms were refined anisotropically. Hydrogen atoms were placed in ideal positions and refined as riding atoms. All non-hydrogen atoms were refined with anisotropic displacement parameters. Final crystallographic parameters and basic information pertaining to data collection and structure refinement are summarized in Table S1. Selected bond lengths (Å) and bond angles (degree) are listed in Table S2. All figures were drawn using MERCURY V 3.0[S5] and DIAMOND V 3.2.[S6]

(S1) (a) Gupta, V; Mandal, S. K. Coordination driven self-assembly of [2 + 2 + 2] molecular squares: synthesis, crystal structures, catalytic and luminescence properties. *Dalton Trans*., **2018**, *47*, 9742-9754. (b) Gupta, V.; Khullar, S.; Kumar, S.; Mandal, S. K. Construction of a robust pillared-layer framework based on the rare paddlewheel subunit $[Mn_2^{II}(\mu\text{-}O_2CR)_4L_2]$: synthesis, crystal structure and magnetic properties. *Dalton Trans*., **2015**, *44*, 16778-16784. (c) Khullar. S.; Mandal. S. K. Ancillary ligand assisted self-assembly of coordination architectures of Mn(II): the effect of the N-alkyl group on a tridentate ligand. *Dalton Trans*. **2015**, *44*, 1203–1210.

(S2) APEX2, SADABS and SAINT, *Bruker AXS Inc*., Madison, WI, USA, 2008.

(S3) Sheldrick, G. M. SHELXTL Version 2014/7, *https://shelx.uniac. gwdg.de/SHELX/index.php*.

(S4) Dolomanov, O. V.; Bourhis, L. J.; Gildea, R. J.; Howard J. A. K.; Puschmann, H. OLEX2: a complete structure solution, refinement and analysis program. *J. Appl. Cryst*. **2009**, *42*, 339-341.

(S5) Macrae, C. F.; Bruno, I. J.; Chisholm, J. A.; Edgington, P. R.; McCabe, P.; Pidcock, E.; Rodriguez-Monge, L.; Taylor, R.; van de Streek, J.; Wood, P. A. Mercury CSD 2.0 - New Features for the Visualization and Investigation of Crystal Structures. *J. Appl. Crystallogr*., **2008**, *41*, 466–470.

(S6) Putz, H.; Brandenburg, K. Diamond - Crystal and Molecular Structure Visualization. *http://www.crystalimpact. com/diamond.*

Table S1. Crystallographic Data Collection and Structure Refinement Parameters for **1**.

Chemical Formula	$C_{32}H_{37}CdN_3O_6Si$
Formula Weight (g/mol)	700.13
Temperature (K)	100(2)
Wavelength (Å)	0.71073
Crystal System	orthorhombic
Space Group	$P\ 2_1\ 2_1\ 2$
a (Å)	21.4402(6)
b (Å)	24.0515(5)
c (Å)	6.25270(10)
α (°)	90
β (°)	90
γ (°)	90
Z	4
V (Å^3)	3224.32(12)
Density (g/cm^3)	1.442
μ(mm^{-1})	0.761
F(000)	1440
Theta (°) Range for Data Coll.	1.27 to 25.06
Reflections Collected	30642
Independent Reflections	5731
Reflections with I >2σ(I))	5475
R_{int}	0.0281
No. of Parameters refined	393
GOF on F^2	1.073
Final R_1[a]/wR_2[b] (I >2σ(I))	0.0298/0.0672
Weighted R_1/wR_2(all data)	0.0319/0.0679
Largest diff. peak and hole(eÅ^{-3})	0.505 -0.317

[a] $R_1 = \Sigma||F_o| - |F_c||/\Sigma|F_o|$. [b] $wR_2 = [\Sigma w(F_o^2 - F_c^2)^2/\Sigma w(F_o^2)^2]^{1/2}$, where $w = 1/[\sigma^2(F_o^2) + (aP)^2 + bP]$, $P = (F_o^2 + 2F_c^2)/3$

Table S2. Selected bond lengths (Å) and angles (º) for **1**.

1			
Cd1-O1	2.456(3)	Cd1-O2	2.350(3)
Cd1-O3	2.410(3)	Cd1-O4	2.415(3)
Cd1-O5	2.308(3)	Cd1-N1	2.324(5)
Cd1-N2	2.354(4)	O5-H5A	0.8607
O5-H5B	0.8621	N3-C30	1.422(8)
N3-C31	1.449(8)	N3-C32	1.337(8)
C32-O6	1.212(8)	O5-Cd1-N1	91.22(19)
O5-Cd1-O2	85.90(12)	N1-Cd1-O2	91.54(14)
O5-Cd1-N2	88.03(17)	N1-Cd1-N2	177.68(15)
O2-Cd1-N2	86.22(13)	O5-Cd1-O3	138.17(12)
N1-Cd1-O3	90.31(16)	O2-Cd1-O3	135.84(11)
N2-Cd1-O3	91.72(14)	O5-Cd1-O4	84.33(12)
N1-Cd1-O4	98.84(12)	O2-Cd1-O4	165.88(13)
N2-Cd1-O4	83.27(12)	O3-Cd1-O4	54.18(12)
O5-Cd1-O1	139.42(11)	N1-Cd1-O1	84.76(16)
O2-Cd1-O1	53.97(11)	N2-Cd1-O1	94.39(14)
O3-Cd1-O1	82.33(10)	O4-Cd1-O1	136.22(11)
C30-N3-C31	117.3(5)	C32-N3-C30	122.6(6)
C32-N3-C31	119.7(6)	O6-C32-N3	125.9(7)

Symmetry codes:
(#1) 'x, y, z', (#2) 'x+1/2, -y+1/2, -z', (#3) '-x+1/2, y+1/2, -z', (#4) '-x, -y, z'

Table S3. Output results of TOPOS program for topology of 1

```
###################################
1:VG_Cd_bpp_Si2_0ma in P2(1)2(1)2
###################################

Topology for ZE1
--------------------
Atom ZE1 links by bridge ligands and has
Common vertex with                        R(A-A)       f
ZE 1    0.2933    1.4004   -0.0365   ( 0 0 0)    12.177A       1
ZE 1    0.2933    0.4004   -0.0365   ( 0-1 0)    12.177A       1
ZE 1    0.2933    0.4004   -1.0365   ( 0-1-1)    13.895A       1
ZE 1    0.2933    1.4004   -1.0365   ( 0 0-1)    13.895A       1
-------------------------
Structural group analysis
-------------------------

-------------------------
Structural group No 1
-------------------------
Structure consists of layers ( 1 0 0) with ZEZCZB
Num. groups=2; Thickness=4.26; Min.Distance=10.720

Coordination sequences
----------------------
ZE1:  1  2  3  4  5  6   7   8   9  10
Num   4  8 12 16 20 24  28  32  36  40
Cum   5 13 25 41 61 85 113 145 181 221
----------------------
TD10=221

Vertex symbols for selected sublattice
--------------------------------------
ZE1 Point symbol:{4^4.6^2}
Extended point symbol:[4.4.4.4.6(2).6(2)]
--------------------------------------
Point symbol for net: {4^4.6^2}
4-c net; uninodal net
Topological type: sql/Shubnikov tetragonal plane net (topos&RCSR.ttd) {4^4.6^2} - VS [4.4.4.4.*.*]
        (17467 types in 3 databases)

Elapsed time: 10.69 sec
```